



MMB triazole analogues are potent NF- κ B inhibitors and anti-cancer agents against both hematological and solid tumor cells

Venumadhav Janganati,^a Jessica Ponder,^{b,c} Meenakshisundaram Balasubramaniam,^d Poornima Bhat-Nakshatri,^{e,f} Eli E. Bar,^g Harikrishna Nakshatri,^{e,f} Craig T. Jordan,^{b,c} and Peter A. Crooks^{a,*}

^a Department of Pharmaceutical Sciences, College of Pharmacy, University of Arkansas for Medical Sciences, Little Rock, AR 72205, USA; ^b Division of Hematology, University of Colorado, Aurora, CO 80045, USA; ^c Department of Toxicology, University of Colorado, Aurora, CO 80045, USA; ^d Department of Geriatrics, College of Medicine, University of Arkansas for Medical Sciences, Little Rock, AR 72205, USA; ^e Department of Surgery, Indiana School of Medicine, Indianapolis, IN 46202, USA; ^f Department of Biochemistry and Molecular Biology, Indiana School of Medicine, Indianapolis, IN 46202, USA; ^g Department of Neurological Surgery, Case Comprehensive Cancer Center, Case Western Reserve University School of Medicine, USA.

ARTICLE INFO

Article history:

Received
Received in revised form
Accepted
Available online

Keywords:

Melampomagnolide B
Leukemia cell lines
NF- κ B pathway
Click chemistry
Triazole derivatives

ABSTRACT

Triazole derivatives of melampomagnolide B (MMB) have been synthesized via click chemistry methodologies and screened against a panel of 60 human cancer cell lines. Several derivatives showed promising anti-cancer activity, affording growth inhibition (GI_{50}) values in the nanomolar range ($GI_{50} = 0.02\text{--}0.99 \mu\text{M}$). Lead compound **7h** exhibited EC_{50} values of 400 nM and 700 nM, respectively, against two AML clinical specimens. Compound **7h** was significantly more potent than parthenolide as an inhibitor of p65 phosphorylation in both hematological and solid tumor cell lines, indicating its ability to inhibit the NF- κ B pathway. In TMD-231 breast cancer cells, treatment with **7h** reduced DNA binding activity of NF- κ B through inhibition of IKK- β mediated p65 phosphorylation and caused elevation of basal I κ B α levels through inhibition of constitutive I κ B α turnover and NF- κ B activation. Molecular docking and dynamic modeling studies indicated that **7h** interacts with the kinase domain of the monomeric IKK β subunit, leading to inhibition of IKK β activation, and compromising phosphorylation of downstream targets of the NF- κ B pathway; dynamic modeling studies show that this interaction also causes unwinding of the α -helix of the NEMO binding site on IKK β . Molecular docking studies with **10**, a water-soluble analogue of **7h**, demonstrate that this analog interacts with the dimerization/oligomerization domain of monomeric IKK β and may inhibit oligomer formation and subsequent autophosphorylation. Sesquiterpene lactones **7h** and **10** are considered ideal candidates for potential clinical development.

2009 Elsevier Ltd. All rights reserved.

1. Introduction

Anti-cancer sesquiterpene lactones have been isolated from several medicinal plants; for example, parthenolide (PTL) (**Fig. 1**) [1] isolated from feverfew (*Tanacetum parthenium*) and melampomagnolide B (MMB) (**Fig. 1**) from *Magnolia grandiflora* [2], have been the source of several potent anti-cancer sesquiterpene lactone derivatives that are effective against both hematological and solid tumors [3-6]. Sesquiterpene lactones PTL and MMB have both been shown to inhibit the activation of the nuclear factor kappa B (NF- κ B; p65/p50) transcription factor complex, causing a down-regulation of anti-apoptotic genes under NF- κ B control (**Fig. 2**) [7, 8]. Utilizing streptavidin pull-down and LC/MS/MS peptide sequencing methodologies with a novel MMB-biotin conjugate, [9] we have demonstrated that both the inhibitor-of-kappa kinase beta subunit (IKK β) and transcription factor p65 (relA) proteins of the NF- κ B pathway can be identified as potential targets in the mechanism of action of MMB and PTL.

*Corresponding author. Tel.: +1 501 686 6495; fax: +1 501 686 6057. E-mail address: pacrooks@uams.edu (P.A. Crooks).

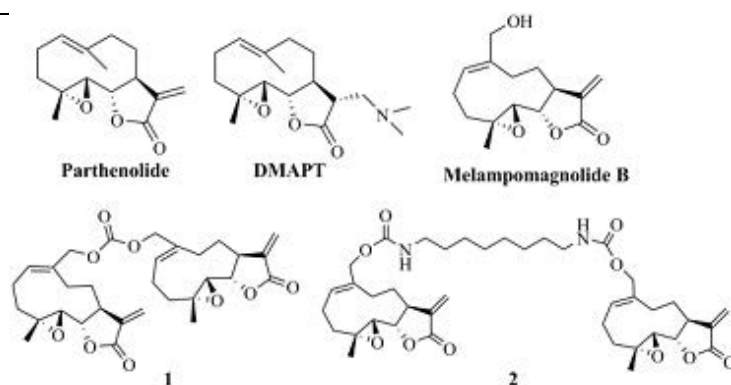


Figure 1: The anti-cancer sesquiterpene lactones parthenolide (PTL), DMAPT, melampomagnolide B (MMB), and MMB carbonate and carbamate dimers **1** and **2**, respectively.

These sesquiterpene lactones are believed to inhibit IKK β mediated phosphorylation of the inhibitor-of-kappaB (I κ B)/p65p50 complex [10]. The I κ B/p65p50 complex represents an inactivated cytoplasmic form of NF- κ B, which prevents nuclear translocation of NF- κ B. In cancer cells, cell membrane-

Graphical Abstract

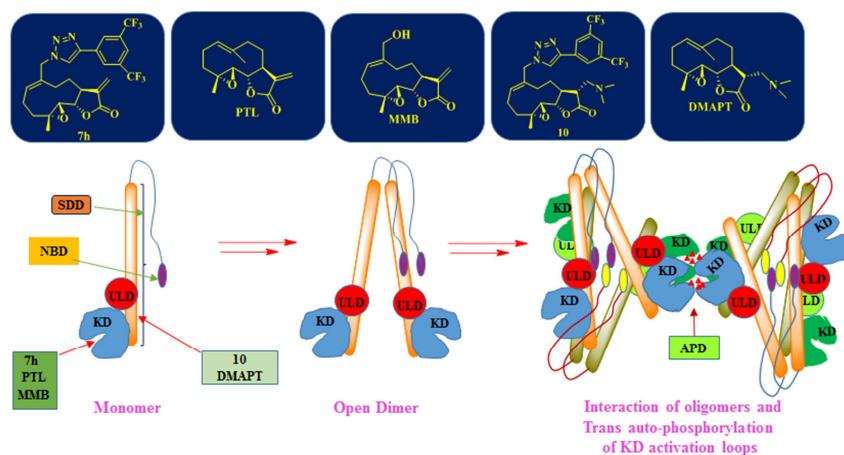
To create your abstract, type over the instructions in the template box below.
 Fonts or abstract dimensions should not be changed or altered.

MMB triazole analogues are potent NF- κ B inhibitors and anti-cancer agents against both hematological and solid tumor cells

Leave this area blank for abstract info.

Venumadhav Janganati,^a Jessica Ponder,^{b,c} Meenakshisundaram Balasubramaniam,^d Poornima Bhat-Nakshatri,^{e,f} Eli E. Bar,^g Harikrishna Nakshatri,^{e,f} Craig T. Jordan,^{b,c} and Peter A. Crooks^{a,*}

^aDepartment of Pharmaceutical Sciences, College of Pharmacy, University of Arkansas for Medical Sciences, Little Rock, AR 72205, USA; ^bDivision of Hematology, University of Colorado, Aurora, CO 80045, USA; ^cDepartment of Toxicology, University of Colorado, Aurora, CO 80045, USA; ^dDepartment of Geriatrics, College of Medicine, University of Arkansas for Medical Sciences, Little Rock, AR 72205, USA; ^eDepartment of Surgery, Indiana School of Medicine, Indianapolis, IN 46202, USA; ^fDepartment of Biochemistry and Molecular Biology, Indiana School of Medicine, Indianapolis, IN 46202, USA. ^gDepartment of Neurological Surgery, Case Comprehensive Cancer Center, Case Western Reserve University School of Medicine, USA.



bound receptors cause activation of IKK β , which then phosphorylates the I κ B/p65p50 complex, releasing phosphorylated I κ B (which is programmed for subsequent ubiquitinylation and proteasomal degradation), and phosphorylated p65p50 (NF- κ B), which can then interact with its DNA binding site to up-regulate anti-apoptotic gene transcription (Fig. 2). During this process, disassociation of I κ B releases the NF- κ B heterodimer inducing its location to the nucleus, where it binds to specific gene promoters that inhibit apoptosis.

The anti-cancer activity of PTL is not solely due to NF- κ B inhibition [7, 11, 12], but rather arises from a broad set of biological responses, which likely include inhibition of components of glutathione biosynthesis and catabolism [13], leading to an increase in reactive oxygen species (ROS) [14]. We have previously shown that PTL perturbs glutathione homeostasis in primary AML stem cells via a multifactorial mechanism, causing an increase in ROS and resulting in promotion of apoptosis (Fig. 2) [14]. Utilization of the MMB-biotin probe in streptavidin pull-down and peptide sequencing studies and homology molecular modeling studies both indicate that the sesquiterpene lactones PTL and MMB target the modulatory (GCLM) and catalytic (GCLC) units of the glutathione-cysteine ligase enzyme (which is the rate-limiting step in glutathione biosynthesis) and the enzymes glutathione peroxidase (GPX1) and thioredoxin (TRX) [14].

studies for evaluation as a treatment for AML and other related leukemias [16]. Several other Michael adducts of PTL have been synthesized and evaluated for their anti-leukemic activity. [17-19]

The sesquiterpene lactone MMB has been the source of several synthetic anti-leukemic molecules arising from our program over the past few years [3-6, 21]. In this respect, MMB can be conveniently synthesized from PTL utilizing a modification of the method of Macias *et al* [20] via a one-step selenium oxide oxidation of the C10 methyl group of PTL to a hydroxymethyl moiety. This reaction occurs with concomitant conversion of the geometry of the C9-C10 bond from *trans* to *cis* [9]. Like PTL, MMB exhibits anti-leukemic properties [9]; however, unlike PTL, the structure of the MMB molecule provides more scope and greater opportunities for generating new chemical space around this interesting sesquiterpene lactone scaffold, since the molecule possesses an allylic hydroxyl group at C-14, which allows the synthesis of new MMB derivatives via conjugation and functional group transformations at this site. Thus, we have used a C-14 biotin-conjugated derivative of MMB for elucidating the mechanism of action of MMB in AML stem cells [9] and we have synthesized a variety of conjugated derivatives of MMB which exhibit potent anti-cancer activity against a wide variety of human cancer cell lines [3-6, 21]. We have also reported on some novel carbamate, and carbonate dimers of MMB (e.g. 1 & 2, Fig. 1), which represent some of the most potent anti-cancer sesquiterpene lactone analogs currently known [4].

Based on these important findings, and to further probe the chemical space around the MMB molecule, in this current study we describe the synthesis of several MMB-1,2,3-triazole derivatives by reaction of a C-14 azido derivative of MMB with a variety of substituted aromatic, heterocyclic and aliphatic acetylenic reagents via click chemistry methodologies. Click chemistry is an important approach for the synthesis of drug-like 1,2,3-triazole compounds and has become one of the most rapid and popular approaches for the synthesis of compound libraries [22, 23]. Employing click chemistry methodologies can accelerate the drug discovery process, since these relatively facile synthetic procedures are usually insensitive to oxygen and water [24], utilize readily available reagents, and incorporate simple isolation methodologies [25, 26].

1,2,3-triazole moieties have been found to be useful heterocyclic structural motifs in medicinal chemistry because of their ease of synthesis. Compounds containing these moieties have been used for a wide variety of pharmacological activities, including antibacterial [27, 28], antifungal [29, 30], antiviral [31, 32], anti-inflammatory [33, 34] and anticancer [35-39] therapy. The triazole moiety contains three nitrogen atoms in a five membered heteroaromatic ring, and its incorporation into a potential drug molecule can play an important role in enhancing anticancer activity through improved water solubility, chemical and metabolic stability, and improved pharmacokinetic properties [36, 40]. Because of their high dipole moment [41] and aromaticity 1,2,3-triazoles can actively participate in hydrogen bonding, and dipole-dipole and π -stacking interactions, which may improve binding with target proteins [42-44]. They are also considered as amide and peptide bond isosteres [45, 46]. A comprehensive review of the medicinal attributes of 1,2,3-triazoles has recently been published [47]. In this current communication, copper I catalysts have been utilized for the synthesis of a variety of 1,2,3-triazole analogs of MMB from appropriate azido and acetylenic precursors. These molecules have been evaluated as anti-cancer agents and their mechanism of action has been investigated.

2. RESULTS AND DISCUSSION

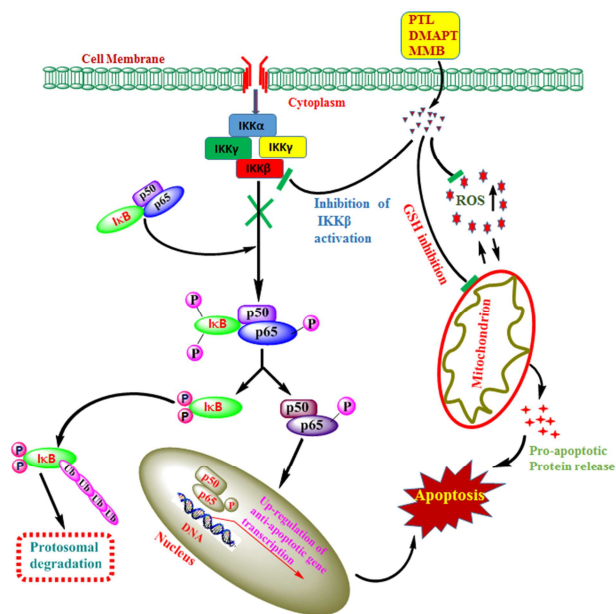
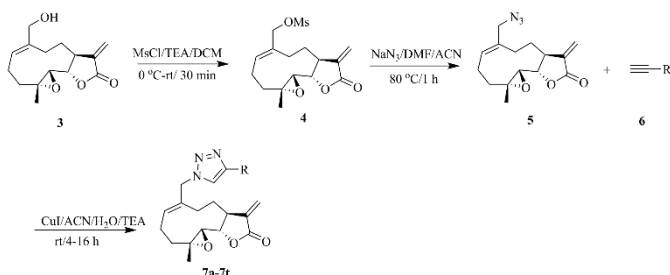


Figure 2: Proposed mechanism of action of the sesquiterpene lactones parthenolide (PTL), DMAPT and melampomagnolide B (MMB): A primary mechanism involves inhibition of IKK β activation, causing decreased phosphorylation of I κ B and/or p65, resulting in down-regulation of anti-apoptotic gene transcription and sensitization of cancer cells to apoptotic signals. A secondary synergistic mechanism involves inhibition of the mitochondrial glutathione system, causing an increase in reactive oxygen species (ROS) and oxidative stress leading to mitochondrial dysfunction and activation of intrinsic apoptosis in cancer cells.

It has previously been demonstrated that PTL induces robust apoptosis of primary acute myeloid leukemia (AML) stem cells. [15, 16] However, PTL suffers from poor water-solubility and low bioavailability. To improve the water-solubility and drug-likeness of PTL we synthesized a dimethylamino analog of parthenolide, DMAPT (Fig. 1), by reaction of PTL with dimethylamine under Michael addition reaction conditions. The water-soluble fumarate salt of DMAPT exhibited similar anti-leukemic activity as PTL [17] and is currently in Phase I clinical

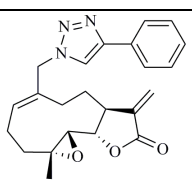
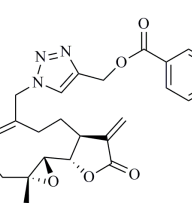
MMB (**3**) was synthesized from PTL via $\text{SeO}_2/\text{tBuOOH}$ oxidation [20]. The MMB mesylate **4** was synthesized by initial reaction of MMB with methane sulfonyl chloride in dichloromethane at 0 °C for 30 min; compound **4** was then reacted with sodium azide in the presence of dimethylformamide and acetonitrile at 80 °C for 1 h to afford the azido synthon **5**. Intermediate **5** was then treated with a variety of aromatic, aliphatic and heteroaromatic acetylenic reagents (**6**) in the presence of $\text{CuI}/\text{triethylamine}/\text{acetonitrile}$ and water (9:1) at ambient temperature to afford the corresponding MMB triazole derivatives **7a-7s** (Scheme 1). Dimeric triazole derivatives of MMB were also synthesized by reaction of an appropriate diacetylenic intermediate (**8**) with azido synthon **5** (Scheme 2).

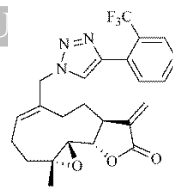
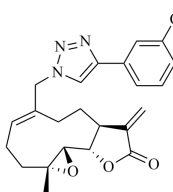
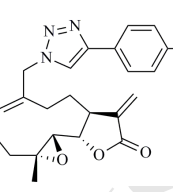
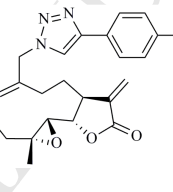
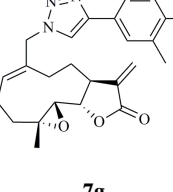
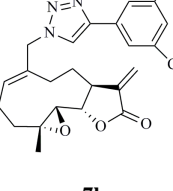
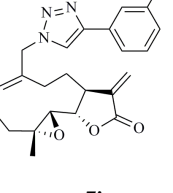
A more water-soluble dimethylamino adduct of compound **7h** was also synthesized; **7h** was reacted with dimethylamine in methanol under Michael addition conditions to afford the corresponding Michael adduct, which was then converted into the fumarate salt **10** with fumaric acid in ethanol (Scheme 3). The water solubility of **10** was predicted to be 1,000 times greater than for **7h** (ACD/Percepta 14.1.0), i.e. 0.11 mg/mL versus 0.00005 mg/mL, respectively. All synthesized compounds were purified by column chromatography (silica gel; methanol/dichloromethane) to afford analytically pure products (Tables 1 & 2) in 57-91% yield. Products were fully characterized by ^1H NMR, ^{13}C NMR and HRMS spectral analysis.

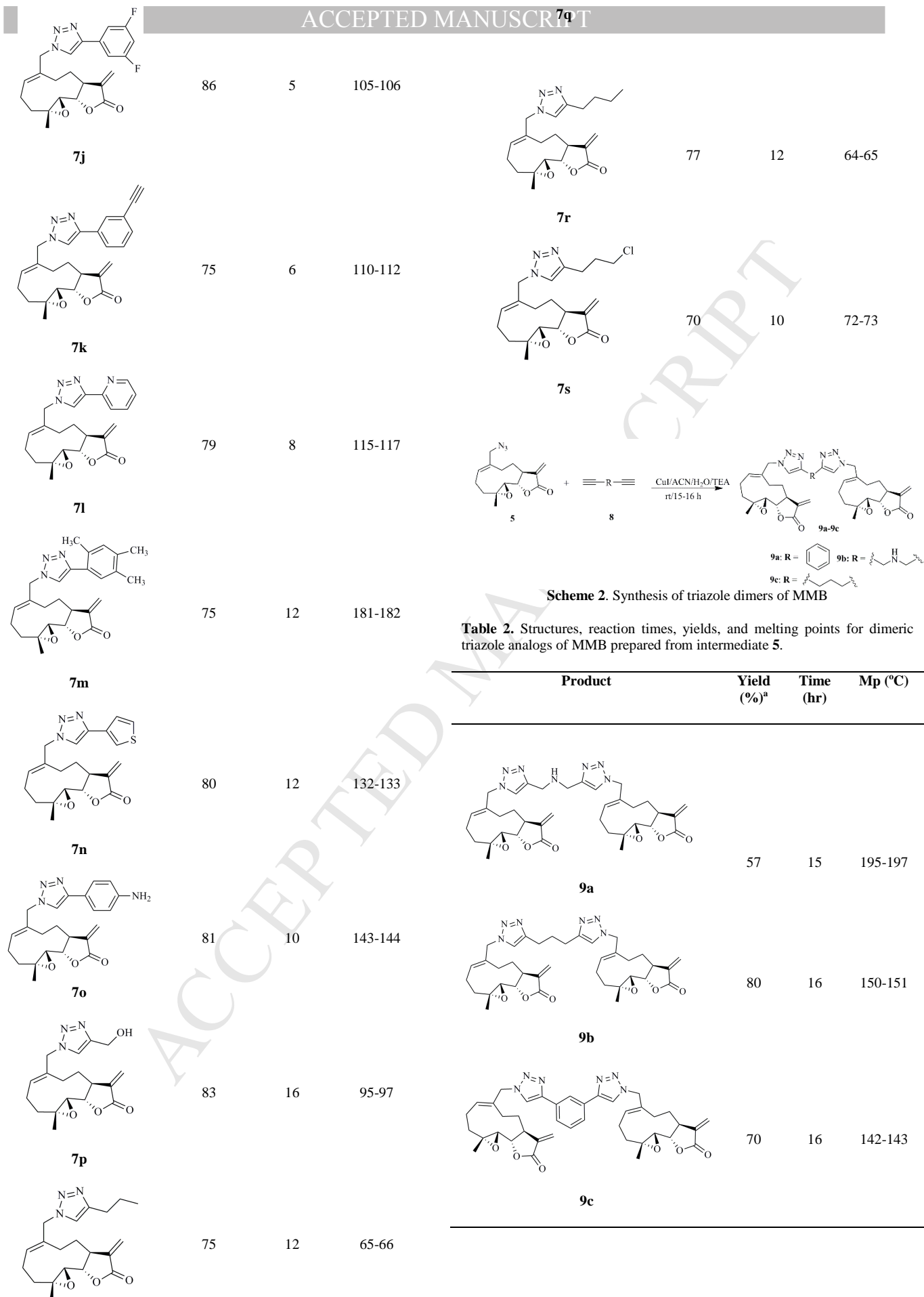


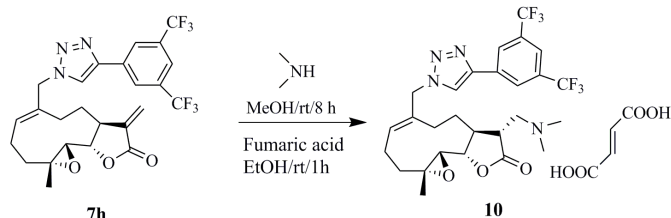
Scheme 1: Synthesis of triazole derivatives of MMB

Table 1. Structures, reaction times, yields, and melting points for triazole derivatives of MMB prepared from intermediate **5**

Product	Yield (%) ^a	Time (hr)	Mp (°C)
	91	6	107-108
	85	10	75-76

	87	6	74-75
	85	8	98-99
	86	8	108-109
	80	8	97-98
	85	8	80-81
	89	4	106-107
	80	6	130-132





Scheme 3. Synthesis of compound **10**, the dimethylamino Michael adduct of **7h**

2.2. BIOLOGICAL ACTIVITY

2.2.1. *In vitro* growth inhibition data against a panel of 60 human cancer cell lines

The above triazole derivatives of MMB were evaluated for growth inhibitory properties against an NCI panel of 60 human cancer cell lines derived from nine cancer cell types, grouped into disease sub-panels that represent leukemia, lung, colon, central nervous system (CNS), melanoma, renal, ovary, breast, and prostate cancer cells. Growth inhibitory (GI_{50}) effects were measured as a function of the variation of optical density as a percentage of control. The compounds were first screened at a single concentration of 10^{-5} M. Compounds which showed more than 60% growth inhibition in at least eight of the sixty cell lines in the panel were selected for a complete dose response study with five different concentrations (10^{-4} M, 10^{-5} M, 10^{-6} M, 10^{-7} M and 10^{-8} M) of drug.

Table 3. Growth inhibition (GI_{50}) data^a for compounds **7a**, **7c-7f**, **7h**, **7m-7o** and **7q** against a panel of 60 human cancer cell lines

Panel/cell line	7a	7c	7d	7e	7f	7h	7m	7n	7o	7q
	GI_{50}^a (μ M)	GI_{50}^a (μ M)	GI_{50}^a (μ M)	GI_{50}^a (μ M)	GI_{50}^a (μ M)	GI_{50}^a (μ M)	GI_{50}^a (μ M)	GI_{50}^a (μ M)	GI_{50}^a (μ M)	GI_{50}^a (μ M)
Leukemia										
CCRF-CEM	0.99	0.76	0.20	0.24	0.29	0.16	0.45	1.63	2.0	3.00
HL-60(TB)	1.49	2.58	0.33	0.72	1.17	0.19	0.64	1.91	2.23	3.53
K-562	1.76	2.40	0.40	0.94	1.30	0.23	1.39	2.51	2.99	3.96
MOLT-4	1.29	3.03	0.31	0.38	1.13	0.19	2.38	2.59	2.87	5.54
RPMI-8226	1.71	1.87	0.50	1.41	1.87	0.22	1.18	2.45	2.75	5.52
SR	1.06	0.81	0.23	0.25	0.25	0.10	1.26	0.56	0.70	2.88
Non-Small Cell Lung Cancer										
A549/ATCC	5.88	7.23	1.79	3.37	10.9	1.36	1.73	8.61	11.9	22.3
EKVX	6.87	2.32	1.57	1.49	2.47	1.50	1.22	2.33	3.89	11.5
HOP-62	7.41	4.73	1.94	3.04	10.5	1.56	1.77	4.90	10.2	14.1
HOP-92	1.42	1.48	0.25	0.34	1.13	0.34	0.43	1.66	2.13	2.94
NCI-H226	4.60	1.73	1.71	2.48	1.99	1.65	1.46	2.09	3.34	12.6
NCI-H23	5.38	1.75	1.58	1.78	2.06	1.12	1.77	1.82	2.49	13.6
NCI-H322M	7.79	10.8	2.17	4.39	10.7	1.67	11.1	10.5	12.6	21.5
NCI-H460	7.74	3.97	2.13	3.66	8.45	1.22	3.16	4.71	10.4	21.2
NCI-H522	0.81	1.38	0.29	0.25	0.38	0.12	0.28	1.39	1.37	3.06
Colon Cancer										

All synthesized compounds were submitted to the NCI screening program and compounds **7a**, **7c-7f**, **7h**, **7m-7o** and **7q**, were selected for single dose screening. Based on the single dose results, all ten compounds were selected for five-dose testing (**Table 3**). Among these compounds, two analogs: **7h** and **7d**, exhibited potent growth inhibition ($GI_{50} < 1\mu$ M) against 66% and 50%, respectively, of all the cell lines in the 60-cell panel. Compounds **7e**, **7f** and **7m** afforded GI_{50} values of $< 1\mu$ M in 40%, 32% and 24% of the cell lines in the panel. Compounds **7h**, **7d**, and **7e** were effective against the 6-cell lines in the leukemia sub-panel, and exhibited GI_{50} values over the ranges 0.10-0.23 μ M, 0.20-0.50 μ M, and 0.24-1.41 μ M, respectively. Compounds **7h**, **7d** and **7e** were also effective anti-cancer agents against the subpanel of human colon cancer cell lines with GI_{50} values over the ranges 0.14-1.17 μ M, 0.16-1.78 μ M and 0.28-1.74 μ M, respectively. Against the nine cell lines in the melanoma subpanel, **7h** and **7d** afforded GI_{50} values of 0.15-1.47 μ M and 0.28-1.70 μ M, respectively. Compounds **7h**, **7d** and **7e** were also potent anti-cancer agents against the eight cell lines in the human renal cancer sub-panel, with GI_{50} values of 0.02-0.70 μ M, 0.18-1.52 μ M, and 0.18-1.82 μ M, respectively. **7h** was particularly effective against the RXF 393 renal cancer cell line with a GI_{50} value of 0.02 μ M and was also a potent anti-cancer agent against the ovarian cancer cell subpanel (GI_{50} 0.15-1.86 μ M), the prostate cancer cell panel (GI_{50} 0.72-0.83 μ M), and the breast cancer cell subpanel (GI_{50} 0.17-1.03 μ M).

COLO 205	1.08	1.98	0.41	0.45	0.50	0.14	0.64	1.45	1.79	5.22
HCC-2998	6.16	1.85	1.64	1.74	1.98	1.17	1.72	1.84	3.49	15.1
HCT-116	1.17	1.26	0.16	0.29	0.48	0.15	0.33	1.16	1.55	3.98
HCT-15	0.77	1.05	0.19	0.28	0.33	0.19	0.20	1.11	1.42	2.90
HT29	1.79	1.79	0.51	0.69	1.23	0.19	0.50	1.66	2.14	5.50
KM12	8.48	5.88	1.78	1.70	3.51	1.04	2.31	6.45	11.4	17.6
SW-620	1.50	1.24	0.33	0.42	0.49	0.19	0.42	1.32	2.16	4.23
CNS Cancer										
SF-268	5.63	2.09	1.59	1.69	2.07	1.08	1.52	2.53	3.70	13.7
SF-295	7.89	10.3	3.41	5.73	11.0	1.19	6.44	9.61	12.1	18.5
SF-539	2.01	1.76	0.25	0.27	0.34	0.17	1.16	1.80	2.77	8.87
SNB-19	7.87	10.8	2.40	3.39	6.92	1.71	3.90	9.49	12.7	18.8
SNB-75	6.21	2.97	1.16	1.25	1.47	1.26	0.52	3.23	4.98	18.5
U251	7.96	1.83	1.61	2.02	9.45	1.44	1.53	2.50	4.16	14.1
Melanoma										
LOX IMVI	0.80	1.11	0.28	0.90	1.16	0.15	0.72	1.28	1.51	3.91
MALME-3M	1.17	1.70	1.20	1.40	1.67	0.52	1.43	1.61	2.18	4.70
M14	1.78	2.15	0.79	0.94	1.30	0.35	1.50	1.93	2.97	3.99
MDA-MB-435	2.37	2.18	0.59	1.00	1.14	0.74	1.41	1.85	3.01	10.4
SK-MEL-2	5.50	2.45	1.66	1.83	1.95	0.34	1.75	2.27	10.6	16.3
SK-MEL-28	1.06	1.75	0.35	0.82	0.82	0.46	1.40	1.81	2.71	ND
SK-MEL-5	7.32	1.72	1.70	1.74	2.10	1.47	1.66	1.83	3.47	15.3
UACC-257	3.78	ND	1.42	1.47	1.78	1.46	1.29	ND	ND	ND
UACC-62	1.87	ND	0.62	1.26	1.35	0.34	1.13	ND	ND	ND
Ovarian Cancer										
IGROV1	6.95	1.81	0.73	1.17	1.35	0.84	1.29	1.92	2.96	4.63
OVCAR-3	1.40	1.04	0.47	0.49	0.56	0.15	1.03	1.06	1.62	3.96
OVCAR-4	3.22	2.77	1.09	1.29	1.52	0.50	0.70	2.48	4.90	9.46
OVCAR-5	5.70	2.46	1.21	1.47	1.71	1.10	1.74	2.29	6.43	14.1
OVCAR-8	2.31	2.23	1.31	1.66	2.59	0.88	0.92	2.96	3.04	13.5
NCI/ADR-RES	6.17	2.99	2.39	3.05	3.08	1.05	2.51	3.79	14.5	15.2
SK-OV-3	9.95	17.3	3.67	9.78	16.3	1.86	11.7	17.4	18.3	26.0
Renal Cancer										
786-0	2.63	1.84	0.50	1.06	1.24	0.16	1.50	1.76	1.98	11.3
A498	7.80	3.86	1.52	1.82	2.35	0.43	1.04	2.65	10.4	21.5
ACHN	0.94	1.45	0.18	0.18	0.29	0.16	1.07	1.32	2.65	3.81
CAKI-1	1.28	1.31	0.86	1.03	1.03	ND	1.08	1.06	1.77	3.91
RXF 393	1.55	1.07	0.55	0.87	0.70	0.02	0.96	1.07	1.41	4.80
SN12C	4.50	2.47	1.40	1.64	1.96	0.70	1.49	2.45	3.48	12.1
TK-10	1.21	1.71	0.99	1.24	1.42	ND	1.46	1.52	2.25	3.86
UO-31	0.87	1.23	1.08	1.22	1.27	0.38	0.52	1.35	1.87	11.1
Prostate Cancer										

PC-3	5.65	4.32	1.98	2.00	9.35	0.83	1.47	4.21	10.1	14.9
DU-145	2.19	1.42	1.00	0.69	1.11	0.72	1.35	1.43	3.65	4.32
Breast Cancer										
MCF7	1.08	1.33	0.31	0.35	0.42	0.19	0.43	1.68	2.41	3.35
MDA-MB-231/ATCC	2.00	1.64	1.09	1.22	1.44	0.33	1.11	1.75	3.45	4.22
HS 578T	9.78	3.57	2.26	3.68	7.42	1.03	1.94	2.82	4.46	23.4
BT-549	2.65	2.40	0.77	0.83	1.31	0.17	0.75	1.80	3.05	14.2
T-47D	1.30	1.70	0.83	0.74	1.43	0.33	0.53	2.03	2.23	4.11
MDA-MB-468	0.95	1.14	0.56	0.42	0.89	0.42	0.53	1.28	1.77	3.65

ND: Not determined; GI₅₀ values <1 μM are bolded; *GI₅₀: 50% growth inhibition defined as concentration of drug resulting in a 50% reduction in net protein increase compared with control cells.

2.2.2. Anti-leukemic activity of MMB triazole analogs **7a-7s**, **9a-9c**, and **10** against M9 ENL1 and primary AML cells

The above triazole derivatives of MMB were screened for anti-leukemic activity against M9 ENL1 and primary AML cell lines; the latter cell lines (AML#1 and AML#2) were obtained with informed consent from AML patients. Evaluations were performed after 24 h of drug exposure using flow cytometric analysis by labeling with Annexin V and 7-aminoactinomycin D (7-AAD) to delineate apoptotic cell populations. For all experiments PTL, MMB and DMAPT were included as reference controls. Depending on the potency of the compound, dose-response curves (0.5-10 μM) were generated to determine the concentration resulting in 50% efficacy (EC₅₀).

Most of the compounds exhibited improved anti-leukemic activity when compared to PTL, MMB and DMAPT (Table 4 and Fig. 3). Compounds **7a**, **7d-7h**, **7j**, and **10** all exhibited anti-leukemic activity against M9 ENL1 cells with EC₅₀ values < 2 μM. The most promising compound was **7h** (EC₅₀ = 0.56 μM), which exhibited 10-fold improvement in potency over PTL (EC₅₀ = 5.9 μM). The above analogs were also cytotoxic to AML#1 and AML#2 primary leukemia cell lines, affording EC₅₀ values in the range 0.4-2.9 μM; again, the most effective compound was **7h** with EC₅₀ values of 0.4 and 0.7 μM, respectively (Table 5, Fig. 4). Compound **7h** was 33-fold and 15-fold more potent than PTL against AML#1 and AML#2 primary cell lines, respectively. Similarly, **7h** was 37-fold and 16-fold more cytotoxic when compared to DMAPT and 51-fold and 35-fold more potent than MMB respectively, against AML#1 and AML#2 primary cell lines. The water-soluble form of **7h**, compound **10**, also exhibited anti-leukemic activity, with EC₅₀ = 1.7, 1.0 and 2.9 μM against M9 ENL1, and primary AML#1 and AML#2 cell lines, respectively. The data show that, as was observed with the conversion of PTL to its equipotent water-soluble analog, DMAPT [17], compound **7h** can also be converted into the water-soluble dimethylamino Michael adduct **10** with retention of the anti-leukemic properties of the parent compound.

Table 4. The anti-leukemic activity of triazole derivatives of MMB against M9 ENL1 AML cells

Compound	M9ENL1 Viability (EC ₅₀ , μM)	95% CI
7a	1.9	[1.6-2.1]

7b	11	[10-12]
7c	3.9	[3.6-4.4]
7d	1.6	[1.5-1.6]
7e	1.7	[1.7-1.8]
7f	1.4	[1.3-1.6]
7g	1.2	[1.1-1.4]
7h	0.56	[0.52-0.60]
7i	>> 10	ND
7j	1.5	[1.54-1.58]
7k	3.3	[3.0-3.6]
7l	3.2	[3.0-3.5]
7m	9.8	[7.0-14]
7n	2.7	[2.6-2.8]
7o	2.8	[2.5-3.1]
7p	38	[32.9-44.7]
7q	5.5	[4.9-6.2]
7r	4.3	[4.0-4.7]
7s	3.8	[3.7-3.9]
9a	>> 10	ND
9b	4.0	[3.9-4.3]
9c	2.3	[2.2-2.4]
10	1.7	[1.3-2.3]
PTL	5.9	[5.4-6.5]
DMAPT	6.9	[6.4-7.3]
MMB	14	[13-15]

^a EC₅₀ values are given in μM. Values below 2 μM are bolded.

Table 5. The anti-leukemic activity of triazole derivatives of MMB against primary AML cell lines

--	--	--

Compound	AML#1 viability ^a (EC ₅₀ , μM)	95% CI	AML#2 viability (EC ₅₀ , μM)	95% CI	7l	5.8	(5.5-6.2)	>10	ND
	1.0	(0.9-1.1)	1.7	(1.6-1.8)	10	2.9	(2.8-3.1)	3.5	(2.7-4.6)
7d	1.0	(0.9-1.1)	1.7	(1.6-1.8)	PTL	7	(5-9)	4.3	(3.8-4.8)
7e	1.1	(1.0-1.3)	1.9	(1.2-2.8)	DMAPT	11	(10-12)	8.2	(7.1-9.5)
7f	2.0	(1.6-2.4)	2.5	(2.2-2.8)	MMB	24	(22-26)	>10	ND
7g	1.3	(1.1-1.4)	1.2	(1.2-1.3)					
7h	0.4	(0.3-0.6)	0.7	(0.7-0.8)					
7j	2.8	(2.5-3.0)	2.5	(2.2-2.8)					

^aEC₅₀ values are given in μM. Values below 2 μM are bolded

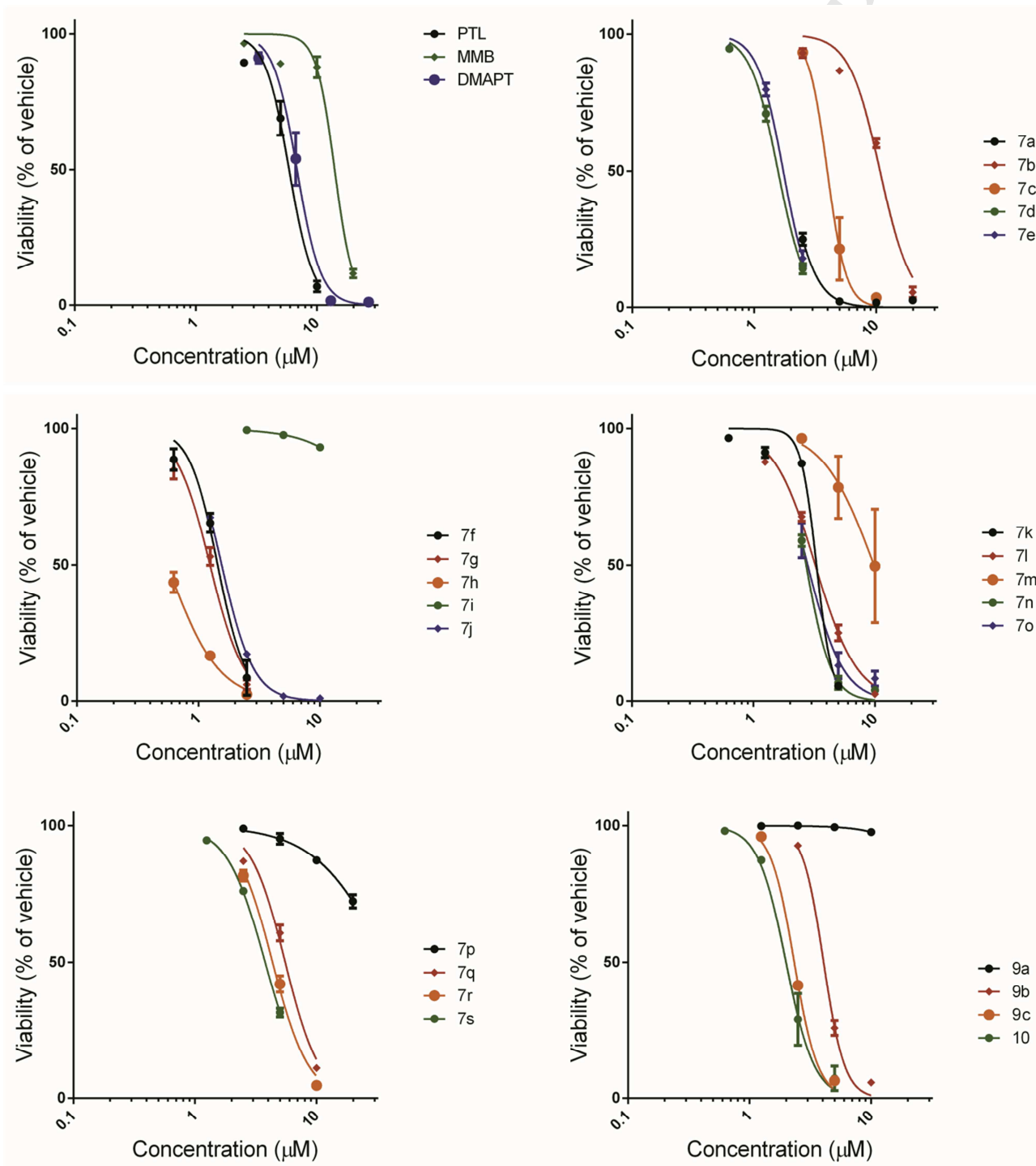


Figure 3: Comparative anti-leukemic activity of PTL, DMAPT, MMB, and compounds **7a-7s**, **9a-9c** and **10** against M9 ENL-1 cells

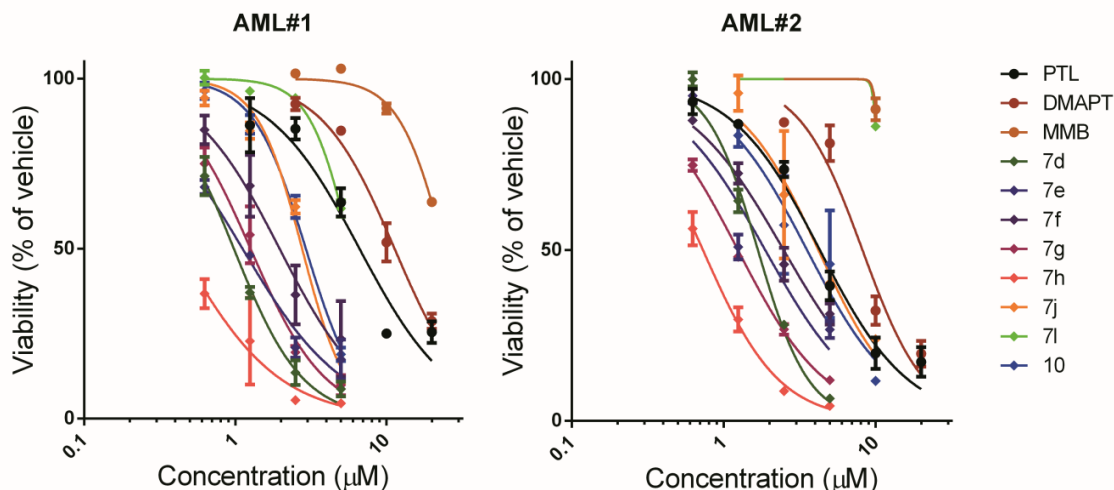
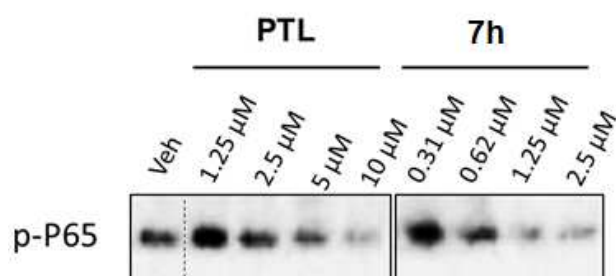


Figure 4: Comparative anti-leukemic activity of PTL, DMAPT, MMB, and compounds **7d-7h**, **7j**, **7l** and **10**, against primary leukemia cells from two AML patients.

In the dimeric series of analogs, compounds **9b** and **9c**, which incorporate 4,4'-(propylene) and 1,3-phenyl linkers, respectively, between the two triazole-MMB units in the molecule, exhibited anti-leukemic activity against M9 ENL1 cells comparable in potency to PTL ($EC_{50} = 4.0$ and $2.3 \mu\text{M}$, respectively). The dimeric analog **9a**, which incorporates a 2-azapropylene unit between the two triazole MMB moieties, showed very poor anti-leukemic potency ($EC_{50} = 52 \mu\text{M}$) (Table 4) against M9 ENL1 cells. From the above data, the cytotoxicity of the 4-phenyl analog **7a** ($EC_{50} = 1.9 \mu\text{M}$) is comparable to that for analogs **7c-7g**, **7k**, and **7o** (EC_{50} s = $0.56-3.9 \mu\text{M}$), indicating that introduction of a variety of aromatic substituents into the 4-phenyl moiety of **7a** has little to no effect on potency. The exception is the 3-carboxylate analog **7i**, which had an EC_{50} value $>10 \mu\text{M}$. Substitution at the 4-position of the phenyl group in **7a** for either a 2-pyridyl (**7l**, $EC_{50} = 3.2 \mu\text{M}$) or a 3-thiophenyl (**7n**, $EC_{50} = 2.7 \mu\text{M}$) moiety also did not significantly affect cytotoxicity. Compound **7h**, which incorporates a 3,5-difluoromethylphenyl moiety at C4 of the triazole ring, is clearly the most potent compound in the series ($EC_{50} = 0.56 \mu\text{M}$) against M9 ENL1 cells. A slight loss of potency is observed with the 4-(3,5-difluorophenyl) analog, **7j** ($EC_{50} = 1.5 \mu\text{M}$). A significant loss in cytotoxicity is seen when the phenyl ring in **7a** is separated from the triazole ring by a linker moiety; i.e. compound **7b**, which has the phenyl ring attached to the MMB triazole ring through an ester linker, is less potent ($EC_{50} = 11 \mu\text{M}$) compared to **7a** ($EC_{50} = 1.9 \mu\text{M}$). Also, somewhat lower potency is observed when the 4-phenyl ring is replaced with aliphatic moieties, e.g. compounds **7p-7s**.

2.2.3. Inhibition of p65 phosphorylation by **7h** in primary cell cultures from AML patients



To determine its functional properties, the activity of **7h** was compared to PTL in assays that measure inhibition of NF- κ B activation. Primary leukemia cells were treated with varying concentrations of PTL and **7h** for 6 h, followed by lysis and analysis by immunoblot. Inhibition of NF- κ B activity was assessed by measuring phosphorylation of the NF- κ B p65 subunit at Ser-536. As shown in Fig. 5, a significant loss of p65 phosphorylation is observed in the presence of $2.5 \mu\text{M}$ **7h**, and for PTL at $10 \mu\text{M}$, indicating that **7h** is a more potent inhibitor of p65 phosphorylation compared to PTL in this primary leukemia cell line.

2.2.4. Effect of **7h** and **10** on oxidative stress in primary cells from AML patients

The comparative effects of PTL and **7h** on glutathione (GSH) and oxidized glutathione (GSSG) levels in primary leukemia cells (AML#2) (Fig. 6) were determined. Compound **7h** was less effective than PTL as an inducer of oxidative stress, and dose response studies indicated that although compound **7h** significantly reduced GSH levels at doses of 2.5 and $5 \mu\text{M}$, it had less effect on GSSG levels at these concentrations. Interestingly, compound **10**, the water-soluble analog of **7h**, had little if any effect on either GSH or GSSG levels (Fig. 6), indicating that introduction of the dimethylamino group into the structure of **7h** via Michael addition chemistry eliminates the oxidative stress component of the parent compound.

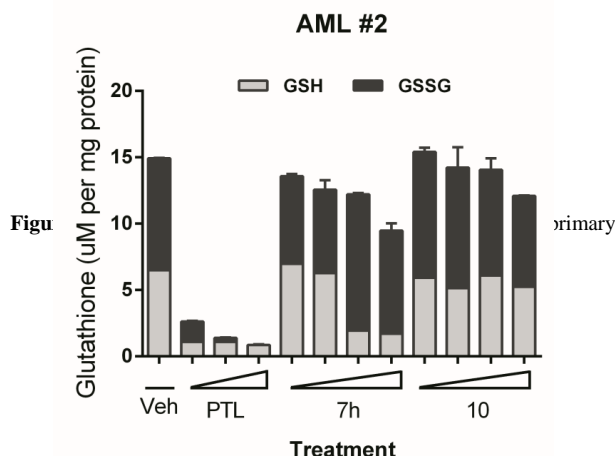


Figure 6: Effect of PTL (2.5, 5 and 10 μM), **7h** (0.625, 1.25, 2.5 and 5 μM), and **10** (0.625, 1.25, 2.5 and 5 μM) on GSH and GSSG levels in primary leukemia cells (AML#2).

2.2.5. Inhibition of HSR-GBM1 stem-like glioblastoma cells by Compound **7h**.

The HSR-GBM1 [48] cell line is representative of glioblastoma multiforme (GBM). This cell line was derived from the NIH-approved H9 (WA09) human ESC line (Invitrogen, Carlsbad, CA, USA) and was cultured as neurospheres on ultra-low attachment plates (Sigma, St. Louis, MO) in DMEM/F12 media containing 2% StemPro neural supplement (both obtained from Gibco, Carlsbad, CA, USA), 20 ng/mL basic fibroblast growth factor (bFGF), and 20 ng/mL epidermal growth factor (EGF); (both obtained from Millipore, Billerica, MA). Cells were passed every 3 days to maintain their undifferentiated state [49]. The most potent MMB triazole analog **7h** was screened for anticancer activity against the HSR-GBM1 cells and exhibited potent anticancer activity in the low micromolar concentration range ($\text{EC}_{50} = 1.11 \mu\text{M}$) (Fig. 7).

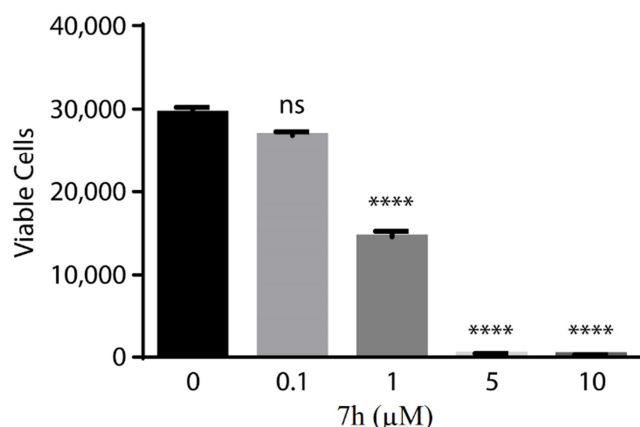


Figure 7: Anti-cancer activity of MMB triazole analog **7h** against HSR-GBM1 stem-like glioblastoma cells. (One-Way ANOVA: **** $p < 0.001$; ns = not significant).

2.2.6. Compound **7h** is a potent inhibitor of NF- κB and cell proliferation in breast cancer cells

The antiproliferative and NF- κB inhibitory effects of **7h** on breast cancer cell lines was determined. Estrogen receptor-positive MCF-7 and estrogen receptor-negative cell lines MDA-MB-231 and MDA-MB-436 were treated with various concentrations of **7h** for 4-5 days, and bromodeoxyuridine incorporation-ELISA assays were used to measure cell proliferation (Fig. 8A). MDA-MB-231 and MDA-MB-436 cell lines used in these experiments are the variants of these cell lines derived from a mammary fat tumor (i.e. TMD-231 and TMD-436). TMD-231 cells showed highest sensitivity to **7h** with a GI_{50} value $< 0.5 \mu\text{M}$, whereas TMD-436 cells were relatively resistant, with a GI_{50} value of $> 1 \mu\text{M}$ (Fig. 8A). Our results suggest that **7h** targets specific signaling pathways in these cancer cell lines to inhibit their proliferation.

Modeling studies suggested that the IKK β subunit is one of the targets of **7h** and thus, **7h** treatment should reduce DNA binding activity of NF- κB , since IKK β activation is required for the release of phosphorylated p65/p50 (NF- κB) from the I $\kappa\text{B}\alpha$ complex. [10] NF- κB demonstrates constitutive DNA binding in TMD-231 cells, likely due to the autocrine action of IL-1 α , [50] and treatment of cells with **7h** for three hours reduced NF- κB DNA binding activity (Fig. 8B). The effect of **7h** is specific to NF- κB , since the drug had no effect on DNA binding of Oct-1. Although the concentration of drug required to inhibit NF- κB DNA binding activity is higher than required to inhibit cell proliferation, duration of drug exposure is different (i.e. three hours versus 4-5 days). Cytokine-mediated NF- κB activation involves activation of IKK β , which phosphorylates and promotes degradation of I $\kappa\text{B}\alpha$. [10]

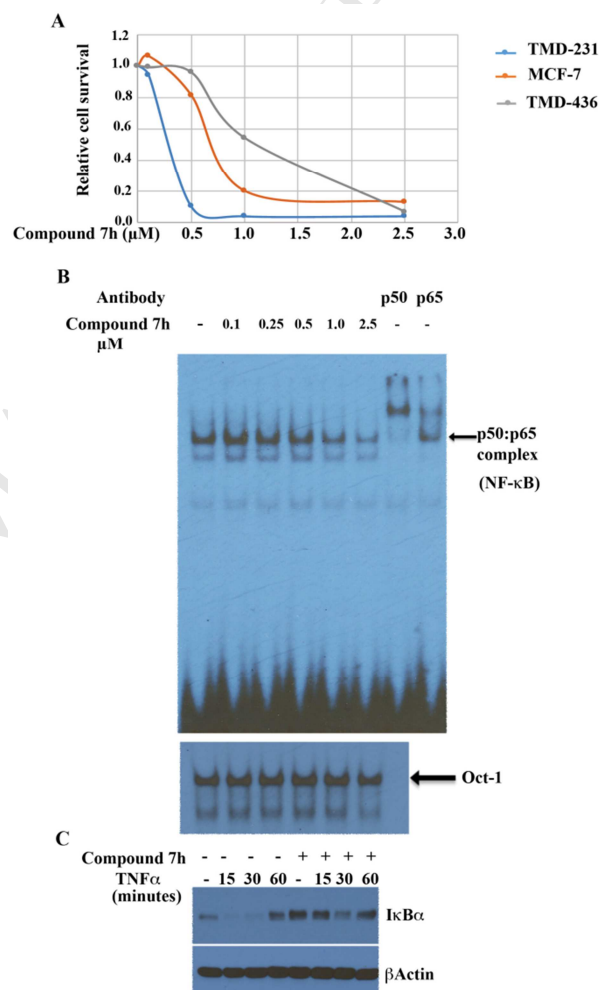


Figure 8: Compound **7h** inhibits cell proliferation and NF- κB . A) The effect of **7h** on proliferation of MDA-MB-231, MCF-7, and MDA-MB-436 breast cancer cell lines. Cells were treated with the indicated concentrations of **7h** and cell proliferation was measured by bromodeoxyuridine ELISA assay 4-5 days after treatment. Results are average values from four experiments, each experiment with six technical replicates. B) Compound **7h** inhibits NF- κB DNA binding activity in TMD-231 cells. Cells were incubated with different concentrations of **7h** for three hours and EMSA was performed to measure NF- κB and Oct-1 DNA binding activity. Antibody supershift assay was used to identify NF- κB subunits in DNA-protein complex (last two lanes). C) Compound **7h** prevents I $\kappa\text{B}\alpha$ degradation. TMD-231 cells were incubated with vehicle or 2.5 μM **7h** for one hour prior to treatment with TNF α (4 ng/mL). Cells were harvested at the indicated time after TNF α treatment and subjected to Western blotting.

We next examined the effect of **7h** pretreatment on TNF α -mediated degradation of I κ B α to confirm the inhibitory effects of **7h** on IKK β . As expected, TNF α treatment caused degradation of I κ B α within 15 minutes, and the protein levels rebounded by one hour (Fig. 8C). In cells pretreated for one hour with 2.5 μ M **7h**, basal I κ B α levels were elevated compared to untreated cells, suggesting the ability of **7h** to inhibit constitutive I κ B α turnover and NF- κ B activation. Consequently, TNF α -mediated cytoplasmic I κ B α degradation was lower in **7h** pretreated cells compared to control cells. These results confirm NF- κ B inhibitory activity of **7h**, and unlike other previously described NF- κ B inhibitors derived from sesquiterpene lactones, compound **7h** is active in the nanomolar range.

2.3. Structure modeling of the IKK β protein

The IKK (I κ B kinase) complex is an essential component for activation of the NF- κ B pathway [51-57]. An activated IKK β subunit is one of the core subunits of the IKK complex, with IKK α , and IKK γ (NEMO) being the other core subunits. IKK α and IKK β are structurally related kinase domain (KD)-containing proteins, whereas NEMO is an obligate scaffolding protein subunit and has a higher affinity for IKK β than for IKK α . Perturbing the activation of IKK β has been shown to have a direct effect on the subsequent activation of NF- κ B and binding of NEMO to IKK β is considered a significant event in activation of the NF- κ B pathway [57-60]. These studies have also shown that inhibiting IKK β -mediated phosphorylation of the I κ B/p65p50 complex prevents activation of NF- κ B and the subsequent upregulation of anti-apoptotic gene transcription. IKK β is an 86 KD protein containing 756 amino acids [30]; it contains four functional domains, namely the KD, the ubiquitin-like domain (ULD), the scaffold/dimerization domain (SDD) and the NEMO binding domain (NBD). Previous studies have determined the importance of each domain in the activation and function of IKK β [28-30]. The KD is one of most studied and important domains in the activation of IKK β , which involves phosphorylation of the key amino acid residues SER 177 & SER 181 present in the activation loop [57]. The ULD is unique, in that it is only found in the IKK β subunit, suggesting an important role for this domain in the activation of NF- κ B. In this respect, it has been shown that ULD deletion mutants of IKK β show poor catalytic activity, and result in loss of NF- κ B activity [61]. Studies have determined that the monomeric IKK β subunit assembles spontaneously and reversibly into dimers and higher order oligomers in solution [30], which is facilitated by the SDD. Although IKK β kinase activity does not depend on dimerization mediated via the SDD, inhibiting IKK β dimerization causes loss of interaction with NEMO, and loss of NEMO interaction can ultimately lead to poor assembly of the

IKK complex and loss of NF- κ B activation [62, 63].

The Results from our previous studies [9,14,15,17], as well as those from the current studies, have shown that the natural sesquiterpene lactones PTL and MMB and their synthetic analogs inhibit the NF- κ B pathway by preventing p65 phosphorylation, and MMB-biotin protein pull-down experiments have identified the IKK β subunit as a target protein [9,14]. Thus, we were particularly interested in determining the mechanism of interaction of the novel MMB-triazole analogs with the IKK β subunit and its relevance to drug design strategies targeting inhibition of IKK β activation. The present molecular modeling study is focused on identifying the mechanism of action of the MMB-triazole analogs as inhibitors of IKK β by studying their interaction with critical domain binding sites on a full length, structural model of the monomeric IKK β subunit.

Since there is no available crystal structure for the complete monomeric form of human IKK β (available crystal structures of IKK β [29-30, 33] lack the NBD region), we modeled a complete monomeric IKK β 3D structure (756 amino acids) that included the missing amino acids of the NBD, using the fold recognition and *ab initio* approach from I-TASSER (<http://zhanglab.ccmb.med.umich.edu/I-TASSER>) [64] (Fig. 9A). We superimposed this predicted structure of monomeric full length IKK β with the monomeric unit in the existing crystal structure of the IKK β dimer (lacking the NBD) (PDB code: 4KIK) [65], and the atomic coordinates of our predicted model, which includes the SDD, KD, and ULD, coincided well with the x-ray crystal structure data (data not shown), indicating the confidence level of the predicted model. Although available crystal structures of IKK β that contain KD binding sites exist in the oligomeric forms [57], the significance of other domains in monomeric IKK β , i.e. the SDD, ULD and NBD, were considered to be of value in determining the mechanism of inhibition of IKK β by **7h** and **10**. Thus, we used the full length monomeric structure of IKK β to determine if the lead MMB-triazole analogs might have the potential to interact with any of the above four domains to inhibit subsequent IKK β oligomerization/activation.

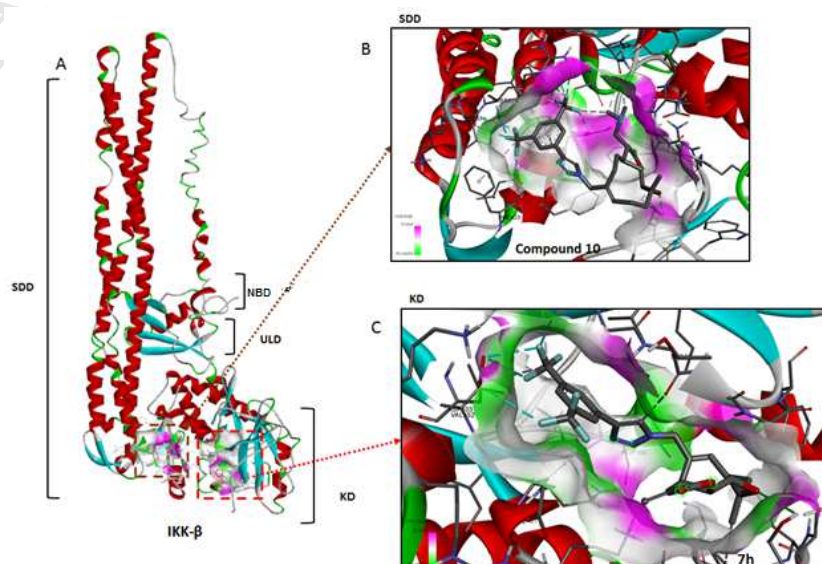


Figure 9: (A) Full length structure of IKK β containing the Kinase Domain (KD), the ubiquitin-like domain (ULD), the Scaffold Dimerization Domain (SDD) and predicted NEMO binding domain (NBD). (B & C) Predicted region of interaction of compounds **7h** and **10**, (B) compound **10** binding to the SDD of IKK β , (C) compound **7h** binding to the KD of IKK β .

3. Molecular docking studies

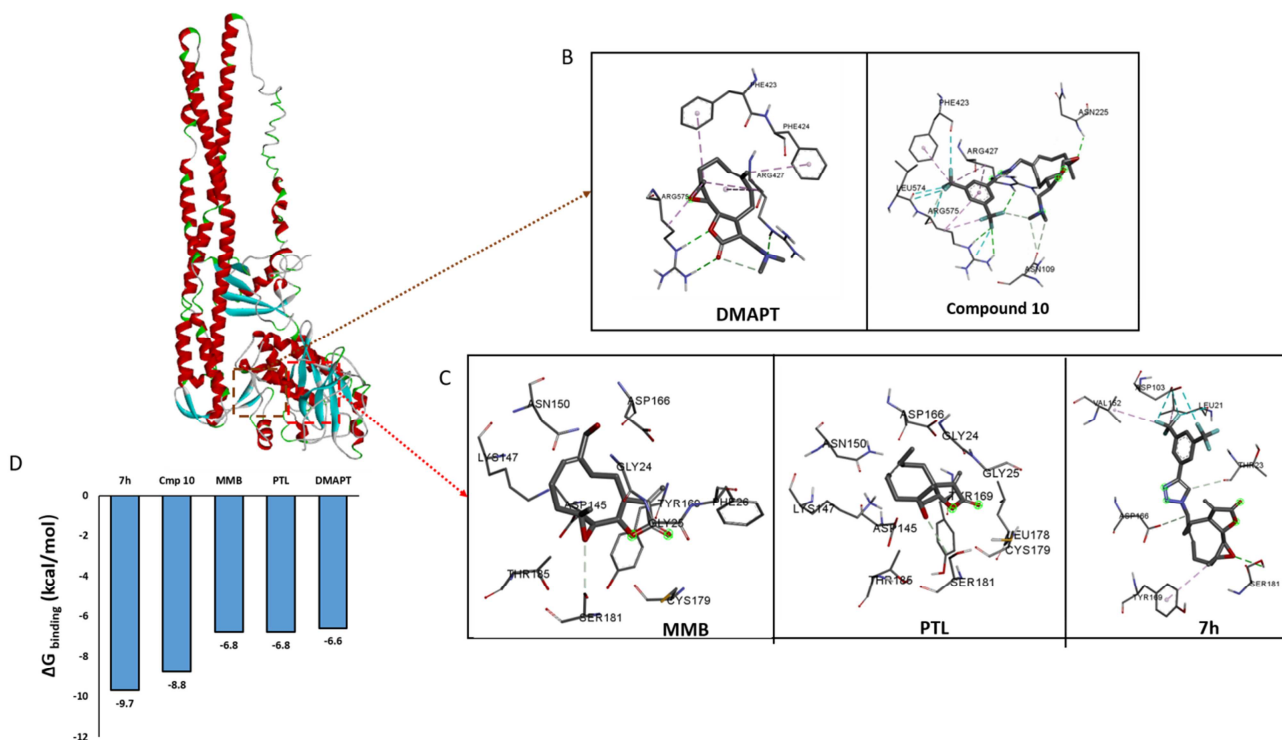


Figure 10: (A) Sites of interaction of compounds screened against IKK β ; (B and C) Predicted site of interaction of MMB, PTL, DMAPT and the MMB-triazole derivatives **7h** and **10**, with full length IKK β : compounds **7h**, MMB, and PTL are predicted to interact with the KD (activation site) of IKK β , whereas DMAPT and compound **10** are predicted to interact at the interface of the SDD and the KD of IKK β (C). (D) Binding free energies of each compound were calculated from Raccoon/AutoDock-Vina [66].

Based on the *in vitro* NCI screening data, the most potent compounds, **7h** and its water-soluble dimethylamino adduct, **10**, together with PTL, DMAPT, and MMB, were selected for docking studies with full length monomeric IKK β , to identify the possible site(s) of action and mechanism(s) of these molecules. Docking calculations were performed in Raccoon/AutoDock-Vina [66] (running on a Linux server). The top ranked (most energetically favorable) docking pose of each molecule and the site of interaction were analyzed in Discovery Studio and LigPlot+ [67]. Molecular docking predicted that all the above compounds bind to IKK β . Interestingly, **7h** and its water-soluble derivative **10** bind to different sites on IKK β (Fig. 9B and 9C). Compound **7h** binds directly to the activation loop (KD) of IKK β and is predicted to inhibit the activation of IKK β by blocking the critical phosphorylation residue SER181 and events leading to inhibition of phosphorylation of other downstream targets, such as I κ B and p65. Compound **10** on the other hand, binds close to the junction between the SDD and the KD. The SDD is a critical domain involved in the dimerization of IKK β . Recent studies support the involvement of a functional dimeric form of IKK β that can exist in a closed and open conformation, the latter conformation allowing subsequent oligomerization to occur through interaction of IKK β monomeric units at neighboring KD sites. Fig. 10A illustrates that **7h**, PTL and MMB both bind to the activation loop of the KD; whereas

compound **10** and DMAPT (a water-soluble analog of PTL) both bind close to the junction between the SDD and the KD sites. Thus, addition of a dimethylamino group at C11 of either the PTL molecule (to afford DMAPT) or to the equivalent site on **7h** (to afford compound **10**) changes the site of interaction of these molecules with IKK β . Interestingly, although DMAPT does not interact with the KD site on IKK β , it is still able to inhibit downstream phosphorylation of p65 [17]. Fig. 10 illustrates the interacting amino acids of IKK β with docked compounds **10** and DMAPT at the SDD site (Fig. 10B) and with docked compounds **7h**, PTL, and MMB at the KD site (Fig. 10C). Activation of IKK β is dependent on phosphorylation of SER 177 and SER 181 [62, 68]. Analyzing the interacting amino acids of IKK β with the docked compounds at the KD site indicates that compounds **7h**, PTL and MMB interact with critical amino acid residues, including SER 177, CYS 179 and SER 181, in a non-covalent fashion. Compound **7h** had the highest binding free energy ($\Delta G_{\text{bind}} = -9.7$ kcal/mol) followed by compound **10**, MMB, PTL and DMAPT (Fig. 10D).

3.1. *in silico* site directed mutagenesis

To determine whether SER181 is a critical residue involved in **7h**-IKK β binding, we performed *in silico* site-directed mutagenesis studies on the modeled IKK β molecule by converting the SER181 amino acid residue to alanine.

Docking of **7h** with mutated IKK β (S181A) afforded less binding affinity compared to IKK β wild type docking, indicating that the presence of SER (probably unmodified) at the 181 position is critical for **7h** binding. Interestingly, when we mutated CYS179 (another critical residue in the kinase domain) to alanine, this change did not affect **7h** binding. Since **7h** possesses an electrophilic exocyclic double bond and is predicted to bind to the CYS179 residue at the KD of IKK β , we wanted to determine whether this molecule could form a covalent bond with the CYS179 residue through Michael adduct formation. We used the Glide-CovDock (covalent docking) module from the Schrodinger small molecule drug discovery suite (Version-2018-1, Schrödinger, LLC, New York, NY, 2018) to predict covalent docking. Out of 10 poses, the lowest energy conformer was chosen based on cDock docking affinity calculations (Table S1, Supporting Information). It was predicted that **7h** undergoes Michael addition at the exocyclic double bond to form a covalent bond with the thiol group of the CYS179 residue. Compound **10** is also predicted to interact with a CYS residue (CYS114) at the interface of the KD and SDD binding sites, but this interaction is not predicted to form a covalent Michael adduct with this amino acid residue. Modeling results also predict that DMAPT may be susceptible to a nucleophilic substitution reaction, either through an interaction at the epoxide ring or at the exocyclic methylene moiety; it is worth noting that the cDock affinity value for DMAPT is lower than that for PTL. Compound **10**, on the other hand, shows very low cDock affinity (-1.994), indicating that its ability to undergo covalent docking is low. Comparing the cDock scores with other molecules, clearly indicates that compound **10** is unlikely to undergo covalent docking with CYS114. Comparing the Autodock (binding score) and cDock scores, it is evident that compound **10** binds to the SDD-KD site very efficiently (Gbind = -8.8 kcal/mol), without forming a covalent bond at the site of binding (cDock score = -1.994). These data are interesting, especially in light of our experimental data indicating that compound **10** does not appear to inhibit the glutathione pathway.

indicating that only SER181 is a critical residue involved in **7h** binding to IKK β . The above *in silico* mutations did not affect the binding of any of the other molecules mentioned in these studies.

3.2 Covalent docking

3.3. Molecular Dynamics simulation of IKK β -**7h** & IKK β -**10** complexes

To analyze the stability of the interaction of **7h** with IKK β , we performed 50ns fully solvated molecular dynamics simulation of IKK β complexed with **7h** (Videos 1 and 2a, Supplementary Data). We also ran an undocked IKK β molecule alone as a control (Video 2b, Supplementary Data). Results (Fig. 11, Panels A and B) indicate stable binding of **7h** to the kinase domain of IKK β and its interaction with amino acid residues SER181 and CYS99 in the simulation. SER181 is one of the key amino acid residues involved in the activation of IKK β [57].

We also studied ligand-induced structural changes to IKK β during the 50ns simulation with **7h**. Interestingly, **7h** induces notable structural changes to IKK β (Fig. 11B, and Video 2a, Supplementary Data). The beta-sheet region near LYS171 unwinds in the presence of **7h** (panel B), indicating that structural changes at the kinase domain of IKK β occur upon **7h** binding. Since **7h** binding is juxtaposed close to SER181, one of the key residues involved in IKK β activation (via phosphorylation of SER181) [57], this MMB analog could be sterically hindering this critical process. Surprisingly, binding of **7h** to the KD of IKK β also induces notable structural changes at the NBD (Fig. 11C); i.e., the majority of the NBD α -helix conformation (red) unwinds when **7h** is bound to the KD (Video 3, Supplementary Information). Since IKK β binds directly to NEMO via the NBD to form the NF- κ B multiprotein complex, and any intervention that leads to failure of NEMO-IKK β binding leads to inhibition of NF- κ B [69], the impact of these **7h**-induced structural changes are notable and

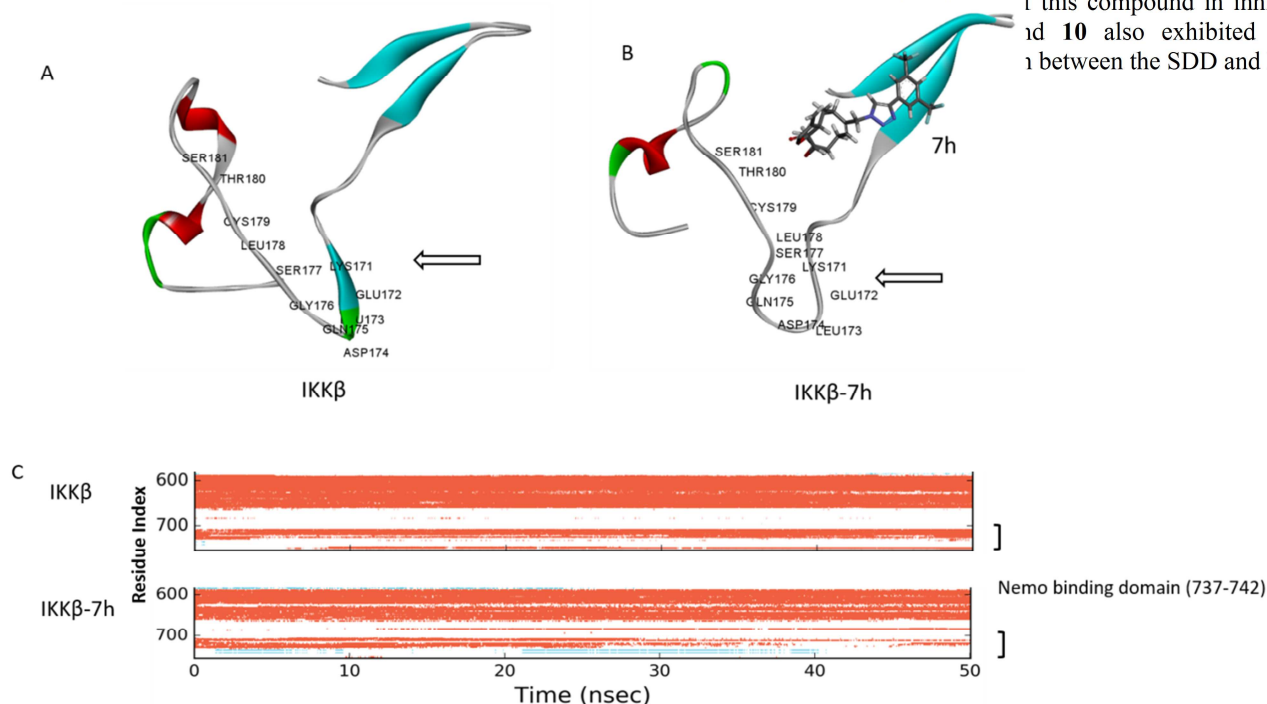
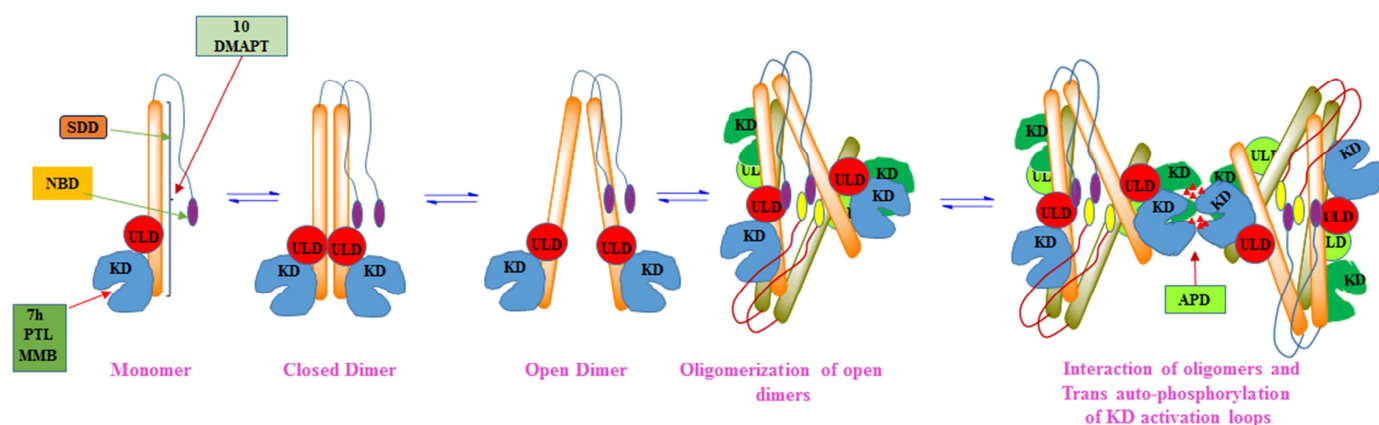


Figure 11: (A & B) Detailed structure of IKK β alone (A) or complexed with **7h** (B) after 50ns simulation. Structures were viewed in Discovery Studio visualizer. (C) Secondary structure assignment over 50ns simulation with IKK β alone (top panel) or when complexed with **7h** (bottom panel), where red indicates beta-sheet, white indicates loops and turns, and blue indicates alpha-helix. Desmond trajectories were analyzed using the simulation interaction diagram module from Maestro (Schrodinger, Inc.).



Abbreviations: NBD: NEMO binding domain; SDD: scaffold dimerization domain; ULD: ubiquitin-like domain; KD: kinase domain; APD: auto phosphorylation domain

Figure 12: Interaction of compounds **7** and **10** with IKK β and the subsequent events in the IKK β oligomerization activation model. Compound **7h** interacts with IKK β at both the NEMO binding domain (NBD) and the kinase domain (KD), blocking transient oligomerization of IKK β and subsequent *trans* autophosphorylation, while inhibition of the scaffold dimerization domain (SDD) by compound **10** results in inhibition of IKK β dimerization and subsequent curtailment of oligomerization.

Although **10** does not induce any major structural changes at this binding site, it does induce moderate structural changes at the SDD by disturbing the helices at several regions of interest (see **Fig. S1** and **Video 3**, Supplementary Information). Also, **10** interacts with amino acid residues that include CYS114 and ARG427, at the junction between the KD and SDD [70]. Since the SDD domain participates in IKK β dimerization, it is likely that compound **10** could inhibit IKK β dimerization and subsequent oligomerization. Studies have shown that dimerization of IKK β plays a critical role for both IKK β activation and NEMO binding [69].

Thus, our molecular docking studies with full length monomeric IKK β indicate that **7h** is predicted to interact with the major activation site (i.e. the KD) on the IKK β -subunit to inhibit the phosphorylation of critical amino acid residues SER177 and SER 181, leading to inhibition of the activation of the IKK β subunit. Also, through molecular dynamics simulation, it is predicted that binding of **7h** at the KD site induces significant structural changes to the monomeric IKK β subunit, which could compromise activation. Surprisingly, compound **10**, the water-soluble analog of **7**, does not retain the oxidative stress component of the parent compound **7h**; also, unlike **7h**, analog **10** is predicted to bind to a different site on the IKK β subunit (i.e. at the junction between the KD and SDD sites, rather than at the KD site), and may inhibit IKK β activity by preventing IKK β dimerization/oligomerization.

We predicted that DMAPT, the water soluble analog of PTL, binds to the same site as **10** on the IKK β subunit, indicating that the *N,N*-dimethylamino adducts of PTL and **7h** are both acting via a different mechanism to their parent compounds. In this respect, it has been hypothesized that these α -methylamino analogs of sesquiterpene lactones might undergo reverse Michael addition *in vivo* through interaction with biological nucleophiles to release the parent sesquiterpene, thereby acting as prodrugs [30, 71-74]. We have previously shown that DMAPT does undergo a reverse Michael reaction in HEPES cell culture buffer, but only 3% conversion to PTL was

observed over 24 hr [17]. This result is consistent with our pharmacokinetic studies with DMAPT fumarate in the rat, which showed that DMAPT has an oral bioavailability of 79%, and is oxidized in the liver to the major *N*-demethylated metabolite, MAPT (methylaminoparthenolide (13-*N*-methyl)amino-4 α 5 β -epoxy-4,10-dimethyl-6 α -hydroxy-12-oic-acid- γ -lactone-germacra-1(10)-ene) with only very small amounts of PTL detected in the plasma over 8 hrs post administration (unpublished data).

To determine the potential of compound **10** to form **7h** via a reverse Michael mechanism, we examined the stability of **10** in aqueous solution ($D_2O/DMSO_{d6}$; pH~7) by NMR spectroscopy over 8 hrs at 37°C and compared it to DMAPT fumarate stability under the same conditions. The results indicate that both DMAPT and **7h** had a slight propensity (2-3%) to undergo a reverse Michael reaction. Thus, we conclude from these data that, as observed with DMAPT fumarate, the anticancer properties of **10** are likely not related to a prodrug mechanism of action for this compound.

Polley et al. [57] have proposed an IKK β oligomerization and activation model in which the open form of monomeric IKK β forms a dimer which can further oligomerize to a dimer of IKK β dimers (tetramer); subsequent oligomerization can then occur to form higher order oligomers that can rapidly amplify IKK β kinase activity through autophosphorylation at adjacent KD interfaces (**Fig. 12**). It has been shown that introduction of mutations within these oligomerization interfaces can disrupt IKK β activation, indicating that small molecule entities designed to bind to these interfaces may function as specific inhibitors of IKK β activation thereby affecting phosphorylation of downstream targets [57, 62]

The proposed sites of action for compounds **7h** and **10** and their parent compounds is illustrated in **Fig. 12**. Based on our docking studies with monomeric IKK β , it is predicted that compound **7h** interacts with the KD and compound **10** interacts with critical amino acid residues at the SDD to inhibit IKK β oligomerization and activation, whereas inhibition of

IKK β dimerization/oligomerization by **10** disrupts subsequent *trans* autophosphorylation of IKK β oligomers. Both mechanisms can result in inhibition of I κ B(p65/p50) phosphorylation, and inhibition of release of NF- κ B from the I κ B(p65/p50) complex, resulting in down-regulation of anti-apoptotic gene transcription and apoptosis of cancer cells.

4. CONCLUSIONS

Triazole derivatives of MMB exhibit improved potency as anti-cancer agents when compared to parent compounds PTL, DMAPT and MMB. The most promising compounds, **7h**, **7d** and **7e**, showed growth inhibition values in the nanomolar range (GI_{50} = 27-990 nm) against many of the human cancer cell lines in the NCI 60 human cancer cell panel. The two most active compounds, **7h** and **7d** afforded sub-micromolar GI_{50} values against 66% and 50%, respectively, of all the cancer cell lines in the panel, and exhibited effective cytotoxicity against all six cell lines in the leukemia subpanel (GI_{50} values of 0.10-0.69 μ M and 0.20-0.50 μ M, respectively). Compound **7h** exhibited promising anti-cancer activity against cell lines in the colon cancer, melanoma, renal cancer, and breast cancer sub-panels, and was a particularly potent anti-cancer agent (GI_{50} = 20 nm) against the RXF 393 renal cancer cell line. The MMB-triazole analogs were also screened for anti-leukemic activity against M9 ENL1 and primary AML cell lines. Most of the compounds exhibited anti-leukemic activity in the nanomolar to low micromolar concentration range. Importantly, **7h** showed nanomolar activity (EC_{50} = 400-700 nm) against both M9 ENL1 and primary AML cell lines. To improve the drug-like properties of compound **7h**, the water-soluble C-11 dimethylamino Michael adduct (**10**) was synthesized and tested for anti-leukemic activity. Compound **10** exhibited similar anti-leukemic activity as **7h** against primary AML cells. These MMB-triazole analogs appear to be superior to PTL, DMAPT and MMB as both anti-leukemic agents and as anti-cancer agents against solid tumors.

In mechanistic studies, **7h** was more potent than PTL as an inhibitor of p65 phosphorylation in both hematological and solid tumor cell lines, indicating improved ability to inhibit the NF- κ B pathway. In TMD-231 breast cancer cells, **7h** reduced DNA binding activity of NF- κ B through inhibition of IKK β activation and subsequent p65 phosphorylation. Compound **7h** also elevated basal I κ B α levels when compared to untreated cells, indicating the ability of this sesquiterpene lactone derivative to inhibit constitutive I κ B α turnover and subsequent NF- κ B activation. Thus, TNF α -mediated I κ B α degradation was lowered in cells pretreated with **7h** compared to control cells. Interestingly, **7h** was less effective than PTL in inducing oxidative stress through inhibition of glutathione levels in primary AML cells, whereas **10** did not exhibit any oxidative stress component in its mechanism.

The MMB-triazole **7h** and its water-soluble analog **10** represent new sesquiterpene lactone analogues that target the IKK β subunit to inhibit phosphorylation of downstream elements of the NF- κ B pathway. They are potent anticancer agents and are regarded as potential candidates for clinical development.

5. EXPERIMENTAL

In the synthesis of triazole derivatives of MMB, all reagents, solvents and chemicals were purchased from Sigma-Aldrich Co. LLC. The synthetic reactions were carried out at ambient temperature and the products were purified by flash column chromatography (silica gel; methanol/dichloromethane) to afford pure compounds in 57-91% yield. Melting points were

recorded on a Kofler hot-stage apparatus and are uncorrected. 1 H and 13 C NMR spectra were recorded on a Varian 400 MHz spectrometer equipped with a Linux workstation running on vNMRj software. All the spectra were phased, baseline was corrected where necessary, and solvent signals (CDCl $_3$) were used as reference for both 1 H and 13 C NMR spectra. Chemical shifts are given as δ values in parts per million (*ppm*) and coupling constants (*J*) are given in hertz (Hz). HRMS data were obtained on an Agilent 6210 LCTOF instrument operating in multimode. Infrared spectra were recorded on a Nicolet iS50 FT-IR spectrometer (Thermo Scientific). Thin-layer chromatographic (TLC) separations were carried out on pre-coated silica gel plates (F 254 Merck). The purity of final compounds was determined to be \geq 95% by high pressure liquid chromatographic (HPLC) analysis on a Model 1290A Agilent HPLC-Diode Array unit utilizing an Altima-C18 column (4.6 \times 250 mm, 5 μ m); a mobile phase of acetonitrile containing 30% Milli Q water at a flow rate of 0.8 mL/min was used. UV detection was at 210 nm.

5.1. Synthetic procedure and analytical data for the azido derivative of melampomagnolide B (**5**)

Triethylamine (0.158 mL, 1.13 mmol) and methane sulfonyl chloride (129.3 mg, 1.13 mmol) were added to a solution of MMB (300 mg, 1.13 mmol) in dichloromethane (5 mL) at 0 $^{\circ}$ C. The reaction mixture was stirred at 0 $^{\circ}$ C for 30 min. After completion of the reaction, water was added, and the mixture was extracted with dichloromethane. The organic layer was washed with water (3 \times 10 mL), dried over Na $_2$ SO $_4$ and concentrated under reduced pressure to afford MMB mesylate (**4**). Sodium azide (136.8 mg, 2.10 mmol) was added to MMB mesylate (360 mg, 1.05 mmol) in acetonitrile/DMF (1:1) (10 mL). The reaction mixture was heated at 80 $^{\circ}$ C for 1 h. After completion of the reaction, the solvent was evaporated under reduced pressure and the crude residue was subjected to column purification (silica gel, 30-40 % EtOAc in hexane) to afford the pure azido analog **5** as a white solid (200 mg, 61%).

1 H NMR (CDCl $_3$, 400 MHz): δ 6.27 (d, *J* = 3.6 Hz, 1H), 5.67 (t, *J* = 8.0 Hz, 1H), 5.55 (d, *J* = 3.6 Hz, 1H), 3.87-3.81 (m, 2H), 3.70 (d, *J* = 13.2 Hz, 1H), 2.85 (d, *J* = 9.6 Hz, 1H), 2.76-2.69 (m, 1H), 2.49-2.16 (m, 6H), 1.74- 1.66 (m, 1H), 1.55 (s, 3H), 1.12 (t, *J* = 12 Hz, 1H) *ppm*. 13 C NMR (CDCl $_3$, 100 MHz) δ 169.3, 138.7, 134.8, 131.3, 120.5, 81.0, 63.4, 60.0, 55.7, 42.8, 36.7, 25.5, 24.2, 23.9, 18.1 *ppm*. FT-IR/ATR 2,089.03 (azido moiety), 1751.33, 1265.41, 1250.56, 1146.55, 988.99, 944.22, 814.25 cm^{-1} . HRMS (ESI) *m/z* calcd for C $_{15}$ H $_{20}$ N $_3$ O $_3$ (M + H) $^+$ 289.1426, found 289.1417.

5.2. General Synthetic procedure and analytical data for the triazole derivatives of MMB (**7a-7s**, **9a-9c**)

To the azido analogue of MMB (**5**, 60 mg, 0.20 mmol) in acetonitrile and water (9:1) (3 mL), was added the appropriate acetylenic reagent (0.248 mmol), copper iodide (3.8 mg, 0.02 mmol) and trimethylamine (0.20 mmol). The reaction mixture was stirred for 4-16 h. After completion of the reaction the solvent was evaporated under reduced pressure to afford a crude reaction mass. Water was added to this crude reaction mass, and the mixture extracted with EtOAc. The organic layer was washed with water (2 \times 5 mL), dried over anhydrous Na $_2$ SO $_4$, filtered, and the solvent was evaporated under vacuum to afford the crude reaction product. The crude product was purified by column chromatography (silica gel, 2-5% methanol in dichloromethane) to afford the appropriate triazole derivative of MMB (yield: 57-91 %).

5.2.1 (1aR,7aS,10aS,10bS,E)-1a-Methyl-8-methylene-5-((4-phenyl-1H-1,2,3-triazol-1-yl)methyl)-2,3,6,7,7a,8,10a,10b-octahydrooxireno[2',3':9,10]cyclodeca[1,2-b]furan-9(1aH)-one (7a).

¹H NMR (CDCl₃, 400 MHz): δ 7.84 (d, *J* = 8 Hz, 2H), 7.73 (s, 1H), 7.43 (t, *J* = 7.2 Hz, 2H), 7.34 (t, *J* = 7.2 Hz, 1H), 6.32 (d, *J* = 3.2 Hz, 1H), 5.80 (t, *J* = 8.8 Hz, 1H), 5.70 (d, *J* = 3.2 Hz, 1H), 5.26 (d, *J* = 14.4 Hz, 1H), 4.78 (d, *J* = 14.8 Hz, 1H), 3.86 (t, *J* = 9.2 Hz, 1H), 2.89-2.79 (m, 2H), 2.72-2.62 (m, 1H), 2.48-2.17 (m, 4H), 2.01 (d, *J* = 15.6 Hz, 1H), 1.70-1.62 (m, 1H), 1.54 (s, 3H), 1.16 (t, *J* = 11.2 Hz, 1H) ppm. ¹³C NMR (CDCl₃, 100 MHz) δ 169.2, 148.5, 138.3, 135.3, 132.3, 130.4, 129.0, 128.5, 125.8, 121.7, 119.1, 80.9, 63.5, 59.9, 55.0, 42.7, 36.6, 25.3, 24.2, 23.6, 18.0 ppm. HRMS (ESI) *m/z* calcd for C₂₃H₂₆N₃O₃ (M + H)⁺ 392.1969, found 392.1976.

5.2.2. (1-(((1aR,7aS,10aS,10bS,E)-1a-Methyl-8-methylene-9-oxo-1a,2,3,6,7,7a,8,9,10a,10b-decahydrooxireno[2',3':9,10]cyclodeca[1,2-b]furan-5-yl)methyl)-1H-1,2,3-triazol-4-yl)methyl benzoate (7b).

¹H NMR (CDCl₃, 400 MHz): δ 8.05 (d, *J* = 7.2 Hz, 2H), 7.66 (s, 1H), 7.57 (t, *J* = 7.6 Hz, 1H), 7.44 (t, *J* = 8 Hz, 2H), 6.31 (d, *J* = 3.60 Hz, 1H), 5.77 (t, *J* = 8 Hz, 1H), 5.67 (d, *J* = 3.2 Hz, 1H), 5.51-5.43 (m, 2H), 5.20 (d, *J* = 14.4 Hz, 1H), 4.72 (d, *J* = 14.4 Hz, 1H), 3.85 (t, *J* = 9.2 Hz, 1H), 2.86 (d, *J* = 9.2 Hz, 1H), 2.80-2.74 (m, 1H), 2.65-2.56 (m, 1H), 2.46-2.17 (m, 4H), 1.97-1.93 (m, 1H), 1.69-1.61 (m, 1H), 1.53 (s, 3H), 1.14 (t, *J* = 13.2 Hz, 1H) ppm. ¹³C NMR (CDCl₃, 100 MHz) δ 169.2, 166.6, 143.7, 138.2, 134.9, 133.4, 132.7, 129.9, 129.8, 128.5, 123.7, 121.1, 80.9, 63.5, 59.9, 58.1, 55.0, 42.7, 36.6, 25.3, 24.2, 23.6, 18.0 ppm. HRMS (ESI) *m/z* calcd for C₂₅H₂₈N₃O₅ (M + H)⁺ 450.2023, found 450.2001.

5.2.3. (1aR,7aS,10aS,10bS,E)-1a-Methyl-8-methylene-5-((4-(2-(trifluoromethyl)phenyl)-1H-1,2,3-triazol-1-yl)methyl)-2,3,6,7,7a,8,10a,10b-octahydrooxireno[2',3':9,10]cyclodeca[1,2-b]furan-9(1aH)-one (7c)

¹H NMR (CDCl₃, 400 MHz): δ 7.97 (d, *J* = 7.2 Hz, 1H), 7.77 (d, *J* = 8.4 Hz, 1H), 7.72 (s, 1H), 7.65 (t, *J* = 8 Hz, 1H), 7.50 (t, *J* = 7.6 Hz, 1H), 6.32 (d, *J* = 3.2 Hz, 1H), 5.79 (t, *J* = 8.8 Hz, 1H), 5.69 (d, *J* = 3.2 Hz, 1H), 5.25 (d, *J* = 14.4 Hz, 1H), 4.84 (d, *J* = 14.4 Hz, 1H), 3.87 (t, *J* = 9.2 Hz, 1H), 2.89 (d, *J* = 9.2 Hz, 1H), 2.82-2.76 (m, 1H), 2.68-2.59 (m, 1H), 2.51-2.18 (m, 4H), 2.02-1.99 (m, 1H), 1.72-1.64 (m, 1H), 1.55 (s, 3H), 1.19-1.13 (m, 1H) ppm. ¹³C NMR (CDCl₃, 100 MHz) δ 169.3, 144.9, 138.3, 135.1, 132.4, 132.2, 131.7, 128.6, 126.3, 126.2, 122.7, 122.6, 121.1, 80.9, 63.5, 59.9, 55.0, 42.7, 36.6, 25.3, 24.1, 23.7, 18.0 ppm. HRMS (ESI) *m/z* calcd for C₂₄H₂₅F₃N₃O₃ (M + H)⁺ 460.4683, found 460.1908.

5.2.4. (1aR,7aS,10aS,10bS,E)-5-((4-(3-Chlorophenyl)-1H-1,2,3-triazol-1-yl)methyl)-1a-methyl-8-methylene-2,3,6,7,7a,8,10a,10b-octahydrooxireno[2',3':9,10]cyclodeca[1,2-b]furan-9(1aH)-one (7d)

¹H NMR (CDCl₃, 400 MHz): δ 7.81 (s, 1H), 7.74 (d, *J* = 7.6 Hz, 2H), 7.38-7.30 (m, 2H), 6.33 (d, *J* = 3.2 Hz, 1H), 5.81 (t, *J* = 8.0 Hz, 1H), 5.70 (d, *J* = 3.2 Hz, 1H), 5.26 (d, *J* = 14.8 Hz, 1H), 4.78 (d, *J* = 14.4 Hz, 1H), 3.86 (t, *J* = 9.6 Hz, 1H), 2.89-2.79 (m, 2H), 2.69-2.62 (m, 1H), 2.49-2.19 (m, 4H), 2.0 (d, *J* = 14.4 Hz, 1H), 1.67 (t, *J* = 12 Hz, 1H), 1.55 (s, 3H), 1.16 (t, *J* = 11.6 Hz, 1H) ppm. ¹³C NMR (CDCl₃, 100 MHz) δ 169.31, 147.1, 138.3, 135.1, 134.9, 132.4, 132.2, 130.3, 128.4, 125.8, 123.8, 121.1, 119.7, 80.9, 63.4, 59.9, 55.0, 42.7, 36.6, 25.5, 24.2, 23.6, 18.0 ppm. HRMS (ESI) *m/z* calcd for C₂₃H₂₅ClN₃O₃ (M + H)⁺ 426.1579, found 426.1643.

5.2.5. (1aR,7aS,10aS,10bS,E)-5-((4-(4-Fluorophenyl)-1H-2,3-triazol-1-yl)methyl)-1a-methyl-8-methylene-2,3,6,7,7a,8,10a,10b-octahydrooxireno[2',3':9,10]cyclodeca[1,2-b]furan-9(1aH)-one (7e).

¹H NMR (CDCl₃, 400 MHz): δ 7.82-7.78 (m, 2H), 7.69 (s, 1H), 7.12 (t, *J* = 8.8 Hz, 2H), 6.32 (d, *J* = 2.80 Hz, 1H), 5.80 (t, *J* = 8.4 Hz, 1H), 5.69 (d, *J* = 3.2 Hz, 1H), 5.25 (d, *J* = 14.4 Hz, 1H), 4.77 (d, *J* = 14.4 Hz, 1H), 3.86 (t, *J* = 9.6 Hz, 1H), 2.89-2.79 (m, 2H), 2.69-2.63 (m, 1H), 2.49-2.18 (m, 4H), 2.01 (d, *J* = 15.6 Hz, 1H), 1.70-1.63 (m, 1H), 1.54 (s, 3H), 1.16 (t, *J* = 11.6 Hz, 1H) ppm. ¹³C NMR (CDCl₃, 100 MHz) δ 169.2, 164.1, 161.6, 147.6, 138.3, 135.3, 132.3, 127.6, 127.5, 126.7, 126.6, 121.1, 118.9, 116.1, 115.9, 80.9, 63.5, 59.9, 55.0, 42.7, 36.6, 25.2, 24.2, 23.6, 18.0 ppm. HRMS (ESI) *m/z* calcd for C₂₃H₂₅FN₃O₃ (M + H)⁺ 410.1874, found 410.1987.

5.2.6. (1aR,7aS,10aS,10bS,E)-5-((4-(4-Methoxyphenyl)-1H-1,2,3-triazol-1-yl)methyl)-1a-methyl-8-methylene-2,3,6,7,7a,8,10a,10b-octahydrooxireno[2',3':9,10]cyclodeca[1,2-b]furan-9(1aH)-one (7f)

¹H NMR (CDCl₃, 400 MHz): δ 7.76 (d, *J* = 8.8 Hz, 2H), 7.63 (s, 1H), 6.97 (d, *J* = 8.8 Hz, 2H), 6.32 (d, *J* = 3.2 Hz, 1H), 5.79 (t, *J* = 8.0 Hz, 1H), 5.69 (d, *J* = 2.8 Hz, 1H), 5.24 (d, *J* = 14.8 Hz, 1H), 4.75 (d, *J* = 14 Hz, 1H), 3.88-3.84 (m, 4H), 2.89-2.79 (m, 2H), 2.74-2.63 (m, 1H), 2.48-2.18 (m, 4H), 2.01 (d, *J* = 15.6 Hz, 1H), 1.65 (t, *J* = 12.4 Hz, 1H), 1.54 (s, 3H), 1.15 (t, *J* = 14.4 Hz, 1H) ppm. ¹³C NMR (CDCl₃, 100 MHz) δ 169.3, 159.8, 148.2, 138.3, 135.3, 132.1, 127.1, 123.1, 121.1, 118.4, 114.4, 80.9, 63.4, 59.9, 55.4, 54.9, 42.7, 36.6, 25.2, 24.1, 23.6, 18.0 ppm. HRMS (ESI) *m/z* calcd for C₂₄H₂₈N₃O₄ (M + H)⁺ 422.2074, found 422.2128.

5.2.7. (1aR,7aS,10aS,10bS,E)-5-((4-(4-Fluoro-3-methylphenyl)-1H-1,2,3-triazol-1-yl)methyl)-1a-methyl-8-methylene-2,3,6,7,7a,8,10a,10b-octahydrooxireno[2',3':9,10]cyclodeca[1,2-b]furan-9(1aH)-one (7g)

¹H NMR (CDCl₃, 400 MHz): δ 7.69 (d, *J* = 8.4 Hz, 1H), 7.58 (t, *J* = 5.2 Hz, 1H), 7.05 (t, *J* = 8.8 Hz, 1H), 6.3 (d, *J* = 3.2 Hz, 1H), 5.79 (t, *J* = 8.4 Hz, 1H), 5.69 (d, *J* = 2.8 Hz, 1H), 5.25 (d, *J* = 14.4 Hz, 1H), 4.76 (d, *J* = 14.4 Hz, 1H), 3.86 (t, *J* = 9.6 Hz, 1H), 2.89-2.78 (m, 2H), 2.73-2.69 (m, 1H), 2.48-2.18 (m, 8H), 2.01 (d, *J* = 15.2 Hz, 1H), 1.70 (t, *J* = 15.2 Hz, 1H), 1.54 (s, 3H), 1.16 (t, *J* = 12.8 Hz, 1H) ppm. ¹³C NMR (CDCl₃, 100 MHz) δ 169.3, 162.6, 160.2, 147.7, 138.3, 135.2, 132.2, 129.0, 128.9, 126.3, 125.6, 125.4, 124.8, 124.7, 121.1, 118.9, 115.7, 115.4, 80.9, 63.4, 59.9, 54.9, 42.7, 36.6, 25.2, 24.1, 23.7, 18.0, 14.7 ppm. HRMS (ESI) *m/z* calcd for C₂₄H₂₇FN₃O₃ (M + H)⁺ 424.2031, found 424.2076.

5.2.8. (1aR,7aS,10aS,10bS,E)-5-((4-(3,5-bis(Trifluoromethyl)phenyl)-1H-1,2,3-triazol-1-yl)methyl)-1a-methyl-8-methylene-2,3,6,7,7a,8,10a,10b-octahydrooxireno[2',3':9,10]cyclodeca[1,2-b]furan-9(1aH)-one (7h)

¹H NMR (CDCl₃, 400 MHz): δ 8.29 (s, 2H), 7.91 (s, 1H), 7.84 (s, 1H), 6.33 (d, *J* = 3.6 Hz, 1H), 5.83 (t, *J* = 8 Hz, 1H), 5.71 (d, *J* = 2.8 Hz, 1H), 5.31 (d, *J* = 14.8 Hz, 1H), 4.82 (d, *J* = 14.8 Hz, 1H), 3.87 (t, *J* = 9.2 Hz, 1H), 2.89-2.81 (m, 2H), 2.69-2.62 (m, 1H), 2.51-2.20 (m, 4H), 1.99 (d, *J* = 10.4 Hz, 1H), 1.69 (t, *J* = 11.6 Hz, 1H), 1.55 (s, 3H), 1.17 (t, *J* = 10 Hz, 1H) ppm. ¹³C NMR (CDCl₃, 100 MHz) δ 169.2, 145.7, 138.2, 134.9, 132.7, 132.6, 132.6, 132.3, 125.7, 124.6, 121.9, 121.8, 121.1, 120.4, 80.9, 63.4, 59.9, 55.2, 42.7, 36.5, 25.2, 24.2, 23.6, 18.0 ppm. HRMS (ESI) *m/z* calcd for C₂₅H₂₄F₆N₃O₃ (M + H)⁺ 528.1716, found 528.1795.

5.2.9. 3-(1-(((1aR,7aS,10aS,10bS,E)-1a-Methyl-8-methylene-9-oxo-1a,2,3,6,7,7a,8,9,10a,10b-decahydrooxireno[2',3':9,10]cyclodeca[1,2-b]furan-5-yl)methyl)-1H-1,2,3-triazol-4-yl)benzoic acid (7i)

¹H NMR (CDCl₃, 400 MHz): δ 8.47 (s, 1H), 8.21 (d, *J* = 7.6 Hz, 1H), 8.10 (d, *J* = 8 Hz, 1H), 7.87 (s, 1H), 7.57 (t, *J* = 7.6 Hz, 1H), 6.32 (d, *J* = 2.8 Hz, 1H), 5.82 (t, *J* = 8.8 Hz, 1H), 5.70 (d, *J* = 3.2 Hz, 1H), 5.29 (d, *J* = 16 Hz, 1H), 4.81 (d, *J* = 14.4 Hz, 1H), 3.87 (t, *J* = 9.2 Hz, 1H), 2.90-2.81 (m, 2H), 2.72-2.17

(m, 5H), 2.03-1.99 (m, 1H), 1.72-1.64 (m, 1H), 1.55 (s, 3H), 1.20-1.14 (m, 1H) ppm. ¹³C NMR (CDCl₃, 100 MHz) δ 170.9, 169.4, 147.2, 138.3, 135.0, 132.4, 130.9, 130.8, 130.2, 130.0, 129.3, 127.4, 121.1, 120.1, 81.0, 63.4, 60.0, 55.0, 42.6, 36.5, 25.2, 24.1, 23.7, 18.0 ppm. HRMS (ESI) m/z calcd for C₂₄H₂₆N₃O₅ (M + H)⁺ 436.1867, found 436.1958.

5.2.10. (1aR,7aS,10aS,10bS,E)-5-((4-(3,5-Difluorophenyl)-1H-1,2,3-triazol-1-yl)methyl)-1a-methyl-8-methylene-2,3,6,7,7a,8,10a,10b-octahydrooxireno[2',3':9,10]cyclodeca[1,2-b]furan-9(1aH)-one (7j)
¹H NMR (CDCl₃, 400 MHz): δ 7.75 (s, 1H), 7.38-7.33 (m, 2H), 6.78 (t, J = 9.2, 2.4 Hz, 1H), 6.32 (d, J = 3.2 Hz, 1H), 5.81 (t, J = 8 Hz, 1H), 5.69 (d, 1H), 5.26 (d, J = 14.8 Hz, 1H), 4.78 (d, J = 14.4 Hz, 1H), 3.87 (t, J = 9.2 Hz, 1H), 2.89 (d, J = 9.6 Hz, 1H), 2.85-2.79 (m, 1H), 2.71-2.60 (m, 1H), 2.50-2.19 (m, 4H), 2.0 (d, J = 14.4 Hz, 1H), 1.71-1.64 (m, 1H), 1.55 (s, 3H), 1.16 (t, J = 10.8 Hz, 1H) ppm. ¹³C NMR (CDCl₃, 100 MHz) δ 169.3, 164.8, 162.3, 146.4, 138.2, 135.0, 133.6, 132.4, 121.1, 120.2, 108.7, 103.8, 80.9, 63.3, 60.0, 54.9, 42.6, 36.5, 25.2, 24.1, 23.7, 18.0 ppm. HRMS (ESI) m/z calcd for C₂₃H₂₄F₂N₃O₃ (M + H)⁺ 428.1780, found 428.1817.

5.2.11. (1aR,7aS,10aS,10bS,E)-5-((4-(3-Ethynylphenyl)-1H-1,2,3-triazol-1-yl)methyl)-1a-methyl-8-methylene-2,3,6,7,7a,8,10a,10b-octahydrooxireno[2',3':9,10]cyclodeca[1,2-b]furan-9(1aH)-one (7k)
¹H NMR (CDCl₃, 400 MHz): δ 7.91 (s, 1H), 7.88 (d, J = 7.20 Hz, 1H), 7.75 (s, 1H), 7.47 (d, J = 7.6 Hz, 1H), 7.40 (t, J = 7.6 Hz, 1H), 6.32 (d, J = 3.2 Hz, 1H), 5.80 (t, J = 8 Hz, 1H), 5.70 (d, J = 2.8 Hz, 1H), 5.26 (d, J = 14.8 Hz, 1H), 4.77 (d, J = 14.4 Hz, 1H), 3.86 (t, J = 9.6 Hz, 1H), 3.10 (s, 1H), 2.89-2.79 (m, 2H), 2.66-2.61 (m, 1H), 2.48-2.19 (m, 4H), 2.0 (d, J = 15.6 Hz, 1H), 1.70-1.63 (m, 1H), 1.54 (s, 3H), 1.21-1.11 (m, 1H) ppm. ¹³C NMR (CDCl₃, 100 MHz) δ 169.2, 147.5, 138.2, 135.2, 132.4, 132.0, 130.7, 129.4, 129.1, 126.1, 122.8, 121.1, 119.5, 83.3, 80.9, 77.8, 63.4, 59.9, 55.0, 42.7, 36.6, 25.2, 24.2, 23.6, 18.0 ppm. HRMS (ESI) m/z calcd for C₂₅H₂₆N₃O₃ (M + H)⁺ 416.1969, found 416.1931.

5.2.12. (1aR,7aS,10aS,10bS,E)-1a-Methyl-8-methylene-5-((4-(pyridin-2-yl)-1H-1,2,3-triazol-1-yl)methyl)-2,3,6,7,7a,8,10a,10b-octahydrooxireno[2',3':9,10]cyclodeca[1,2-b]furan-9(1aH)-one (7l)
¹H NMR (CDCl₃, 400 MHz): δ 8.57 (d, J = 3.2 Hz, 1H), 8.19 (d, J = 8 Hz, 1H), 8.12 (s, 1H), 7.80 (t, J = 8 Hz, 1H), 7.26-7.23 (m, 1H), 6.32 (d, J = 3.6 Hz, 1H), 5.83 (t, J = 8.4 Hz, 1H), 5.69 (d, J = 2.8 Hz, 1H), 5.26 (d, J = 14.4 Hz, 1H), 4.79 (d, J = 14.4 Hz, 1H), 3.86 (t, J = 9.6 Hz, 1H), 2.89 (d, J = 9.6 Hz, 1H), 2.84-2.78 (m, 1H), 2.68-2.59 (m, 1H), 2.47-2.18 (m, 4H), 2.01 (d, J = 14.8 Hz, 1H), 1.70-1.63 (m, 1H), 1.54 (s, 3H), 1.15 (t, J = 12.8 Hz, 1H) ppm. ¹³C NMR (CDCl₃, 100 MHz) δ 169.2, 150.1, 149.5, 148.9, 138.3, 137.1, 134.8, 132.7, 123.1, 121.6, 121.0, 120.3, 80.9, 63.3, 59.9, 54.9, 42.6, 36.5, 25.2, 24.1, 23.5, 18.0 ppm. HRMS (ESI) m/z calcd for C₂₂H₂₅N₄O₃ (M + H)⁺ 393.1921, found 393.1950.

5.2.13. (1aR,7aS,10aS,10bS,E)-1a-Methyl-8-methylene-5-((4-(2,4,5-trimethylphenyl)-1H-1,2,3-triazol-1-yl)methyl)-2,3,6,7,7a,8,10a,10b-octahydrooxireno[2',3':9,10]cyclodeca[1,2-b]furan-9(1aH)-one (7m)
¹H NMR (CDCl₃, 400 MHz): δ 7.56 (s, 2H), 7.04 (s, 1H), 6.31 (s, 1H), 5.79 (t, J = 8.0 Hz, 1H), 5.69 (s, 1H), 5.25 (d, J = 14.4 Hz, 1H), 4.79 (d, J = 14.4 Hz, 1H), 3.86 (t, J = 9.6 Hz, 1H), 2.89 (d, J = 9.2 Hz, 1H), 2.83-2.65 (m, 2H), 2.48-2.20 (m, 13H), 2.04-1.95 (m, 1H), 1.66 (t, J = 15.2 Hz, 1H), 1.55 (s, 3H), 1.16 (t, J = 13.2 Hz, 1H) ppm. ¹³C NMR (CDCl₃, 100 MHz) δ 169.3, 147.9, 138.3, 136.9, 135.4, 134.4, 132.6, 132.4, 132.1, 129.9, 127.0, 121.1, 120.9, 80.9, 63.5, 59.9, 54.9, 42.7, 36.6, 25.3, 24.2, 23.8, 20.9, 19.5, 19.3, 18.0 ppm. HRMS (ESI) m/z calcd for C₂₆H₃₂N₃O₃ (M + H)⁺ 434.2438, found 434.2462.

5.2.14. (1aR,7aS,10aS,10bS,E)-1a-Methyl-8-methylene-5-((4-(thiophen-3-yl)-1H-1,2,3-triazol-1-yl)methyl)-2,3,6,7,7a,8,10a,10b-octahydrooxireno[2',3':9,10]cyclodeca[1,2-b]furan-9(1aH)-one (7n)
¹H NMR (CDCl₃, 400 MHz): δ 7.69 (d, J = 3.6 Hz, 1H), 7.63 (s, 1H), 7.45 (d, J = 5.2 Hz, 1H), 7.40-7.38 (m, 1H), 6.31 (d, J = 3.6 Hz, 1H), 5.78 (t, J = 8.4 Hz, 1H), 5.69 (d, J = 3.2 Hz, 1H), 5.24 (d, J = 14.4 Hz, 1H), 4.76 (d, J = 14.8 Hz, 1H), 3.86 (t, J = 9.2 Hz, 1H), 2.88-2.78 (m, 2H), 2.70-2.61 (m, 1H), 2.47-2.18 (m, 4H), 2.0-1.95 (m, 1H), 1.70-1.61 (m, 1H), 1.54 (s, 3H), 1.5 (t, J = 12.8 Hz, 1H) ppm. ¹³C NMR (CDCl₃, 100 MHz) δ 169.3, 144.5, 138.3, 135.2, 132.1, 131.7, 126.5, 125.8, 121.3, 121.0, 119.1, 80.9, 63.3, 59.9, 54.8, 42.6, 36.5, 25.2, 24.1, 23.6, 18.0 ppm. HRMS (ESI) m/z calcd for C₂₁H₂₄N₃O₃S (M + H)⁺ 398.1533, found 398.1561.

5.2.15. (1aR,7aS,10aS,10bS,E)-5-((4-(4-Aminophenyl)-1H-1,2,3-triazol-1-yl)methyl)-1a-methyl-8-methylene-2,3,6,7,7a,8,10a,10b-octahydrooxireno[2',3':9,10]cyclodeca[1,2-b]furan-9(1aH)-one (7o)
¹H NMR (CDCl₃, 400 MHz): δ 7.61 (d, J = 9.2 Hz, 2H), 7.56 (s, 1H), 6.72 (d, J = 8.4 Hz, 2H), 6.29 (d, J = 3.2 Hz, 1H), 5.76 (t, J = 8.4 Hz, 1H), 5.67 (d, J = 2.8 Hz, 1H), 5.20 (d, J = 14.4 Hz, 1H), 4.72 (d, J = 14.4 Hz, 1H), 3.83 (t, J = 9.6 Hz, 1H), 2.87-2.78 (m, 2H), 2.70-2.58 (m, 1H), 2.46-2.16 (m, 4H), 1.98-1.94 (m, 1H), 1.68-1.58 (m, 1H), 1.52 (s, 3H), 1.13 (t, J = 13.6 Hz, 1H) ppm. ¹³C NMR (CDCl₃, 100 MHz) δ 169.3, 148.7, 146.8, 138.3, 135.3, 132.0, 127.0, 121.1, 120.8, 117.9, 115.3, 80.9, 63.4, 59.9, 54.9, 42.7, 36.6, 25.2, 24.1, 23.6, 18.0 ppm. HRMS (ESI) m/z calcd for C₂₃H₂₇N₄O₃ (M + H)⁺ 407.2078, found 407.2115.

5.2.16. (1aR,7aS,10aS,10bS,E)-5-((4-(Hydroxymethyl)-1H-1,2,3-triazol-1-yl)methyl)-1a-methyl-8-methylene-2,3,6,7,7a,8,10a,10b-octahydrooxireno[2',3':9,10]cyclodeca[1,2-b]furan-9(1aH)-one (7p)
¹H NMR (CDCl₃, 400 MHz): δ 7.51 (s, 1H), 6.31 (d, J = 3.2 Hz, 1H), 5.76 (t, J = 8.4 Hz, 1H), 5.68 (d, J = 3.2 Hz, 1H), 5.20 (d, J = 14.4 Hz, 1H), 4.82 (d, J = 5.6 Hz, 2H), 4.73 (d, J = 14.8 Hz, 1H), 3.85 (t, J = 8.8 Hz, 1H), 2.87-2.75 (m, 2H), 2.65-2.56 (m, 1H), 2.47-2.18 (m, 4H), 2.05 (t, J = 6.4 Hz, 1H), 1.98-1.94 (m, 1H), 1.69-1.62 (m, 1H), 1.54 (s, 3H), 1.15 (t, J = 10.8 Hz, 1H) ppm. ¹³C NMR (CDCl₃, 100 MHz) δ 169.2, 148.2, 138.3, 135.1, 132.5, 121.2, 121.1, 80.9, 63.5, 59.9, 56.9, 54.9, 42.7, 36.6, 25.3, 24.1, 23.7, 18.0 ppm. HRMS (ESI) m/z calcd for C₁₈H₂₄N₃O₄ (M + H)⁺ 346.1761, found 346.1776.

5.2.17. (1aR,7aS,10aS,10bS,E)-1a-Methyl-8-methylene-5-((4-propyl-1H-1,2,3-triazol-1-yl)methyl)-2,3,6,7,7a,8,10a,10b-octahydrooxireno[2',3':9,10]cyclodeca[1,2-b]furan-9(1aH)-one (7q)
¹H NMR (CDCl₃, 400 MHz): δ 7.23 (s, 1H), 6.30 (d, J = 3.6 Hz, 1H), 5.73 (t, J = 8.0 Hz, 1H), 5.67 (d, J = 3.2 Hz, 1H), 5.16 (d, J = 14.4 Hz, 1H), 4.69 (d, J = 14.8 Hz, 1H), 3.84 (t, J = 9.2 Hz, 1H), 2.87 (d, J = 9.2 Hz, 1H), 2.77-2.58 (m, 4H), 2.45-2.17 (m, 4H), 1.96-1.91 (m, 1H), 1.74-1.58 (m, 3H), 1.54 (s, 3H), 1.14 (t, J = 11.2 Hz, 1H), 0.96 (t, J = 6.8 Hz, 3H) ppm. ¹³C NMR (CDCl₃, 100 MHz) δ 169.3, 149.0, 138.3, 135.5, 131.9, 121.2, 120.2, 80.9, 63.5, 59.9, 54.8, 42.7, 36.7, 27.8, 25.3, 24.1, 23.8, 22.7, 18.0, 13.9 ppm. HRMS (ESI) m/z calcd for C₂₀H₂₈N₃O₃ (M + H)⁺ 358.2125, found 358.2114.

5.2.18. (1aR,7aS,10aS,10bS,E)-5-((4-Butyl-1H-1,2,3-triazol-1-yl)methyl)-1a-methyl-8-methylene-2,3,6,7,7a,8,10a,10b-octahydrooxireno[2',3':9,10]cyclodeca[1,2-b]furan-9(1aH)-one (7r)
¹H NMR (CDCl₃, 400 MHz): δ 7.22 (s, 1H), 6.30 (d, J = 3.6 Hz, 1H), 5.73 (t, J = 8.0 Hz, 1H), 5.67 (d, J = 3.2 Hz, 1H), 5.15 (d, J = 14.4 Hz, 1H), 4.68 (d, J = 14.4 Hz, 1H), 3.84 (t, J = 9.2

H_z, 1H), 2.87 (d, *J* = 9.6 Hz, 1H), 2.77-2.57 (m, 4H), 2.45-2.17 (m, 4H), 1.96-1.91 (m, 1H), 1.68-1.60 (m, 3H), 1.53 (s, 3H), 1.42-1.33 (m, 2H), 1.14 (t, *J* = 11.6 Hz, 1H), 0.93 (t, *J* = 7.6 Hz, 3H) ppm. ¹³C NMR (CDCl₃, 100 MHz) δ 169.3, 149.2, 138.3, 135.4, 131.9, 121.1, 120.1, 80.9, 63.4, 59.9, 54.7, 42.7, 36.6, 31.6, 25.5, 25.3, 24.1, 23.7, 22.4, 18.0, 13.9 ppm. HRMS (ESI) *m/z* calcd for C₂₁H₃₀N₃O₃ (M + H)⁺ 372.2282, found 372.2301.

5.2.19. (1*aR*,7*aS*,10*aS*,10*bS*,*E*)-5-((4-(3-Chloropropyl)-1*H*-1,2,3-triazol-1-yl)methyl)-1*a*-methyl-8-methylene-2,3,6,7,7*a*,8,10*a*,10*b*-octahydrooxireno[2',3':9,10]cyclodeca[1,2-*b*]furan-9(1*aH*)-one (7*s*)

¹H NMR (CDCl₃, 400 MHz): δ 7.30 (s, 1H), 6.30 (d, *J* = 3.2 Hz, 1H), 5.74 (t, *J* = 8.4 Hz, 1H), 5.67 (d, *J* = 2.8 Hz, 1H), 5.16 (d, *J* = 14.4 Hz, 1H), 4.70 (d, *J* = 14.4 Hz, 1H), 3.85 (t, *J* = 8.8 Hz, 1H), 3.57 (t, *J* = 6.0 Hz, 2H), 2.90-2.84 (m, 3H), 2.76 (t, *J* = 9.2 Hz, 1H), 2.64-2.57 (m, 1H), 2.46-2.13 (m, 6H), 1.94 (d, *J* = 8.8 Hz, 1H), 1.64 (t, *J* = 11.2 Hz, 1H), 1.53 (s, 3H), 1.14 (t, *J* = 12.4 Hz, 1H) ppm. ¹³C NMR (CDCl₃, 100 MHz) δ 169.3, 147.1, 138.3, 135.3, 132.1, 121.1, 120.8, 80.9, 63.4, 59.9, 54.8, 44.3, 42.7, 36.6, 31.8, 25.2, 24.1, 23.7, 22.8, 18.0 ppm. HRMS (ESI) *m/z* calcd for C₂₀H₂₇ClN₃O₃ (M + H)⁺ 392.1735, found 392.1738.

5.2.20. (1*aR*,1*a'R*,4*E*,4'*E*,7*aS*,7*a'S*,10*aS*,10*bS*,10*a'S*,10*b'S*)-5,5'-((4,4'-(Azanediylobis(methylene))bis(1*H*-1,2,3-triazole-4,1-diyl))bis(methylene))bis(1*a*-methyl-8-methylene-2,3,6,7,7*a*,8,10*a*,10*b*-octahydrooxireno[2',3':9,10]cyclodeca[1,2-*b*]furan-9(1*aH*)-one) (9*a*).

¹H NMR (CDCl₃, 400 MHz): δ 7.52 (s, 2H), 6.29 (d, *J* = 3.2 Hz, 2H), 5.74 (t, *J* = 7.6 Hz, 2H), 5.6 (d, *J* = 2.8 Hz, 2H), 5.15 (d, *J* = 14.4 Hz, 2H), 4.74 (d, *J* = 14.4 Hz, 2H), 3.93 (s, 4H), 3.84 (t, *J* = 9.2 Hz, 2H), 2.85 (d, *J* = 9.2 Hz, 2H), 2.72-2.56 (m, 4H), 2.47-2.16 (m, 8H), 2.04-1.96 (m, 2H), 1.88-1.74 (m, 2H), 1.67-1.58 (m, 2H), 1.53 (s, 6H), 1.14 (t, *J* = 12.4 Hz, 2H) ppm. ¹³C NMR (CDCl₃, 100 MHz) δ 169.3, 146.5, 138.3, 135.0, 132.2, 121.9, 121.0, 80.9, 63.3, 60.0, 54.7, 43.8, 42.6, 36.5, 29.7, 25.2, 24.0, 23.9, 18.0 ppm. HRMS (ESI) *m/z* calcd for C₃₆H₄₆N₇O₆ (M + H)⁺ 672.3504, found 672.3538.

5.2.21. (1*aR*,1*a'R*,4*E*,4'*E*,7*aS*,7*a'S*,10*aS*,10*bS*,10*a'S*,10*b'S*)-5,5'-((4,4'-(Propane-1,3-diyl))bis(1*H*-1,2,3-triazole-4,1-diyl))-bis(methylene))bis(1*a*-methyl-8-methylene-2,3,6,7,7*a*,8,10*a*,10*b*-octahydrooxireno[2',3':9,10]cyclodeca[1,2-*b*]furan-9(1*aH*)-one) (9*b*).

¹H NMR (CDCl₃, 400 MHz): δ 7.35 (s, 2H), 6.27 (d, *J* = 3.6 Hz, 2H), 5.74 (t, *J* = 8 Hz, 2H), 5.67 (d, *J* = 2.8 Hz, 2H), 5.14 (d, *J* = 14.4 Hz, 2H), 4.76 (d, *J* = 14.8 Hz, 2H), 3.83 (t, *J* = 9.2 Hz, 2H), 2.85 (d, *J* = 9.2 Hz, 2H), 2.76 (t, *J* = 7.6 Hz, 4H), 2.68-2.56 (m, 4H), 2.47-2.16 (m, 8H), 2.06-1.97 (m, 4H), 1.66-1.60 (m, 2H), 1.53 (s, 6H), 1.13 (t, *J* = 13.2 Hz, 2H) ppm. ¹³C NMR (CDCl₃, 100 MHz) δ 169.3, 148.1, 138.2, 135.2, 132.3, 121.1, 120.9, 80.9, 63.4, 60.0, 54.9, 42.7, 36.6, 29.3, 25.4, 24.9, 24.1, 18.0 ppm. HRMS (ESI) *m/z* calcd for C₃₇H₄₇N₆O₆ (M + H)⁺ 671.3552, found 671.3567.

5.2.22. (1*aR*,1*a'R*,4*E*,4'*E*,7*aS*,7*a'S*,10*aS*,10*bS*,10*a'S*,10*b'S*)-5,5'-((4,4'-(1,3-Phenylene))bis(1*H*-1,2,3-triazole-4,1-diyl))bis(methylene))bis(1*a*-methyl-8-methylene-2,3,6,7,7*a*,8,10*a*,10*b*-octahydrooxireno[2',3':9,10]cyclodeca[1,2-*b*]furan-9(1*aH*)-one) (9*c*)

¹H NMR (CDCl₃, 400 MHz): δ 8.30 (s, 1H), 7.86 (s, 2H), 7.82 (d, *J* = 3.2 Hz, 2H), 7.49 (t, *J* = 7.6 Hz, 1H), 6.3 (d, *J* = 3.2 Hz, 2H), 5.81 (t, *J* = 8.4 Hz, 2H), 5.68 (d, *J* = 3.2 Hz, 2H), 5.26 (d, *J* = 14.8 Hz, 2H), 4.81 (d, *J* = 14.4 Hz, 2H), 3.86 (t, *J* = 9.2 Hz, 2H), 2.88 (d, *J* = 9.6 Hz, 2H), 2.84-2.78 (m, 2H), 2.64-2.60 (m, 2H), 2.49-2.19 (m, 10H), 1.70-1.62 (m, 2H), 1.54 (s, 6H), 1.20-1.12 (m, 2H) ppm. ¹³C NMR (CDCl₃, 100 MHz) δ 169.3, 148.0, 138.3, 135.1, 132.5, 131.1, 129.6, 125.5, 122.9, 121.1,

119.7, 80.9, 63.4, 59.9, 55.0, 42.7, 36.6, 25.2, 24.2, 23.7, 18.0 ppm. HRMS (ESI) *m/z* calcd for C₄₀H₄₅N₆O₆ (M + H)⁺ 705.3395, found 705.3472.

5.2.23. (1*aR*,7*aS*,8*R*,10*aS*,10*bS*,*E*)-5-((4-(3,5-bis(Trifluoromethyl)phenyl)-1*H*-1,2,3-triazol-1-yl)methyl)-8-((dimethylamino)methyl)-1*a*-methyl-2,3,6,7,7*a*,8,10*a*,10*b*-octahydro-oxireno[2',3':9,10]cyclodeca[1,2-*b*]furan-9(1*aH*)-one (10)

¹H NMR (CDCl₃, 400 MHz): δ 8.28 (s, 2H), 7.88 (s, 1H), 7.83 (s, 1H), 5.75 (t, *J* = 8 Hz, 1H), 5.68 (d, *J* = 14.4 Hz, 1H), 4.82 (d, *J* = 14.4 Hz, 1H), 3.89 (t, *J* = 9.6 Hz, 1H), 2.90-2.71 (m, 3H), 2.66-2.56 (m, 1H), 2.50-2.17 (m, 12H), 1.87-1.82 (m, 1H), 1.58-1.55 (m, 4H), 1.14 (t, *J* = 13.2 Hz, 1H) ppm. ¹³C NMR (CDCl₃, 100 MHz) δ 176.8, 145.4, 136.0, 132.8, 132.6, 132.2, 131.6, 125.6, 121.9, 121.7, 120.4, 81.2, 64.3, 59.7, 57.5, 54.9, 45.9, 44.3, 41.8, 36.9, 26.4, 24.2, 24.0, 18.0 ppm. HRMS (ESI) *m/z* calcd for C₂₇H₃₁F₆N₄O₃ (M + H)⁺ 573.2295, found 573.2307.

5.3. Methodology for the *in vitro* 60 human cancer cell screening assay

Anti-cancer activity screening against the panel of 60 human cancer cell lines was carried out at the National Cancer Institute utilizing a reported literature procedure [75]. Briefly, RPMI 1640 medium with 5% fetal bovine serum and 2 mM L-glutamine was used for growing the NCI-60 human tumor cells. Initially the tumor cells were inoculated into 96-well microtiter plates in 100 μL of medium at plating densities starting from 5,000 to 40,000 cells per well. The range of cell numbers is dependent on the doubling time of the individual tumor cell lines. The plates were then incubated at 37 °C for 24 hours prior to addition of the submitted compounds. After 24 h, two microtiter plates of each tumor cell line were fixed *in situ* with TCA. The optical density reading at this point represents the cell population for each tumor cell line at the time of compound addition (OD_{zero}). The MMB dimers were dissolved in DMSO at 400-fold concentration to the desired final maximum test concentration, and stored at -80 °C. Then, an aliquot part of the frozen concentrate was thawed and diluted to 10⁻⁴ M concentration with medium containing 50 μg/mL gentamicin. A control sample with just DMSO was also prepared. Aliquot parts (100 μL) of the different MMB triazole dilution controls were added to the appropriate microtiter wells containing 100 μL of medium, resulting in the required final drug concentrations of 10⁻⁵ M and 0 M (control). Once the MMB triazoles were added, the microtiter plates were incubated for 48 hrs at 37 °C and 100 % relative humidity.

Cold TCA was used to terminate the assay for adherent cells. Cells were fixed by the addition of 50 μL of cold 50 % (w/v) TCA and further incubated for 1 hr at 4 °C. The supernatant was discarded, and the microtiter plates were splashed five times with water and air dried. Sulforhodamine B (SRB) solution (100 μL) at 0.4 % (w/v) in 1 % acetic acid was added to each well, and plates were incubated for another 10 minutes at room temperature. After SRB staining, free SRB was removed by washing five times with 1 % acetic acid. Bound SRB stain was successively dissolved with 10 mM trizma base, and the optical density was measured at a wavelength of 515 nm.

The growth inhibitory or cytotoxicity effects of the MMB triazoles in the above cellular assay was measured by determining percentage cell growth (PG) inhibition. Optical density (OD) measurements of SRB-derived color just before exposing the cells to the test compound (OD_{zero}) and after 48hrs exposure to the test compound (OD_{test}) or the control

vehicle (ODctrl) were recorded. Also, this methodology can be accessed from the National Cancer Institute database: <http://dtp.nci.nih.gov/branches/btb/ivclsp.html>

5.4. M9 ENL1 cell and primary AML cell assays

MMB triazole analogs were screened for cytotoxicity against the M9 ENL1 cell line and against primary AML specimens as follows: M9 ENL1 cells were plated at a density of 10^6 cells/mL in alpha-MEM culture media (Invitrogen) supplemented with 5% human plasma, 20% FBS, and the cytokines SCF, IL-3, IL-7, and FLT3 (PeproTech). For primary AML specimens, cells were obtained from volunteer donors. Informed consent was obtained in accordance with the Declaration of Helsinki. Cells were isolated from the samples using Ficoll-Paque (GE Healthcare Bio-Sciences, Pittsburgh, PA) density gradient separation. In some cases, cells were cryopreserved in freezing medium of Iscove modified Dulbecco medium (IMDM), 40% fetal bovine serum (FBS), and 10% dimethylsulfoxide (DMSO) or in CryoStor CS-10 (VWR, West Chester, PA). Cells were cultured in serum-free medium (SFM), prepared with Iscove's MDM supplemented with 20% BIT 9500 serum substitute (StemCell Technologies), LDL, and beta-mercaptoethanol, for 1 hour before the addition of the MMB triazole derivatives. Drugs were diluted from a DMSO stock into PBS such that the final concentration of DMSO did not exceed 0.5%. Flow cytometric analysis was performed by co-staining with Annexin V and 7-AAD, according to manufacturer specifications, to identify the percentage of non-apoptotic cells which was defined as the population with negative staining for both labels. The percentage of non-apoptotic cells observed was normalized to that of the vehicle control and dose-response curves were analyzed using GraphPad Prism software to determine EC₅₀ values. All analyses were conducted in triplicate.

5.6. Inhibition of p65 phosphorylation by 7h in primary cells from AML patients

Primary AML cells were exposed to variable concentrations of PTL (1.25, 2.5, 5.0, and 10 μ M) or 7h (0.30, 0.62, 1.25, and 2.5 μ M) for 6h. Cell lysates were obtained and diluted in 5 \times SDS-PAGE sample buffer (10% w/v SDS, 10 mM DDT, 20% glycerol, 0.2 M Tris-HCl, pH 6.8, 0.05% w/v bromophenol blue), and run on 8–10% SDS-PAGE gels. Protein gels were then transferred to PVDF membrane and blocked with 5% milk in 0.1% TBST (20 mM Tris-HCl pH 7.5, 137 mM NaCl, 0.1% Tween 20), followed by incubation with antibodies against p-p65(ser-536) (Cell Signaling).

5.7. Effect of PTL, 7h and 10 on glutathione levels in primary cells from AML patients

Bulk primary human AML cells were cultured and/or treated at 1 million/mL in Iscove's modified Dulbecco's medium-based serum-free media. For drug treatment, cells were preincubated in the media for 1 h before the addition of drugs, and the treatment time was 24 h. Glutathione quantification is based on the principle that reduced glutathione (GSH) and 5,5-dithiobis(2-nitrobenzoic) acid can react and produce free TNB molecules that emit at 412 nm. Therefore, the amount of GSH is directly proportional to the rate of TNB production over time. Briefly, glutathione samples were prepared by lysing primary AML cells in freshly made glutathione assay lysis buffer (16 mM KH₂PO₄, 82 mM K₂HPO₄, 5 mM EDTA, 0.1% Triton X-100, 6 mg/mL of sulfosalicylic acid). Supernatants were collected and used for three measurements: 1) amount of total glutathione (GSH + GSSG) by measuring the rate of TNB production over time; 2) amount of oxidized glutathione

(GSSG) by first derivatizing GSH with 2-vinylpyridine (Sigma) and then measuring the rate of TNB production over time; 3) quantification of total protein with Bradford assay (Bio-Rad). After completing these three measurements, the GSH level is determined using following formula:

$$[\text{GSH}] = [\text{Total glutathione}] - 2 \times [\text{GSSG}].$$

The glutathione level is expressed as nM/mg of total protein.

5.8. Inhibition of HSR-GBM1 stem-like glioblastoma cells by Compound 7h

The HSR-GBM1 (020913) neurosphere cell line was a kind gift from Dr. Angelo Vescovi. Cells were passaged as previously described (Galli et al²⁷). For growth assays, 8,000 cells were plated in each well of a 96-multiwell plate. Following recovery for 24 hours, drug or vehicle (DMSO) were added such that final DMSO concentration was 0.1%. Cell counts were performed 48 hours following the addition of drug using the Guava 5HT flow cytometer and Guava Viacount reagent (Millipore, Billerica, MA). The calculated EC₅₀ value for 7h was 1.11 μ M. One-way ANOVA was performed. **** = $p < 0.001$; ns = not significant.

5.9. Inhibition of NF- κ B and breast cancer cell proliferation by compound 7h

5.9.1. Cell proliferation assays

500-1000 TMD-231 cells were plated in 96-well plates and drug treatment was initiated a day after plating. Each treatment condition contained six wells. After three days of treatment, bromodeoxyuridine incorporation-ELISA was performed as per manufacturer's instructions (Millipore; cat # QIA58-1000TEST). Results presented are from two biological replicates, each condition with six technical replicates.

5.9.2. Electrophoretic mobility shift assay (EMSA)

EMSAs with whole cell lysates using ³²P-radiolabelled probes with NF- κ B and Oct-1 (as a control) binding sites was performed as described previously [50]. Oligonucleotides with NF- κ B and Oct-1 binding sites were purchased from Promega (NF- κ B, Cat# E329A; Oct-1, Cat# E324B). For supershift assays, DNA-protein complexes were incubated with antibody against p65 (Cell Signaling, cat# 3034) and p50 (Millipore, cat # 06-886) subunits for 10 minutes on ice prior to loading.

5.9.3. Western blotting

Cell lysates were prepared using RIPA buffer and were subjected to Western blotting as described previously [76] and probed with I κ B α antibody (Cell Signaling, Cat#: 9242S) and reprobed with antibody against β -actin (Sigma, Cat#: A5441) as a loading control. TNF α was purchased from Peprotech (Cat# 315-01A).

5.10. Molecular modeling

The amino acid sequence of IKK β was retrieved from the Uniprot database (<http://www.uniprot.org/>). For full length three-dimensional structure prediction, the amino acid sequence of IKK β was submitted to the I-TASSER server (<http://zhanglab.ccmb.med.umich.edu/I-TASSER/>). I-TASSER predicts protein structure utilizing the fold recognition and *ab initio* approach. The structure from I-TASSER was then energy-minimized in a cubic box containing water (SPC) and solvent (NaCl) for 5,000 steps using GROMACS simulation package. Energy minimized structures were then used for docking studies.

Protein ligand docking was performed using Autodock-VINA running on a 32 core Linux server with Raccoon2 interface (Windows 7); the grid box was kept large enough to cover the entire protein in order to ensure unbiased docking searches. Although computationally intensive, this method allows compounds to freely choose their binding region. Ligands were converted to autodock format (.pdbqt) using OpenBabel before the docking search. Results from Autodock-VINA were then analyzed in Pymol, and interacting residues were identified using LigPlot+ [67, 77].

5.10.2. Molecular Dynamics Simulation

MD simulations were performed using the Desmond Molecular Dynamics system, version 2016.4, D.E. Shaw Research, New York, NY. The IKK β molecule alone or complexed with **7h** or **10** was first immersed in an orthorhombic solvent box containing SPC water, counter-ions and 0.15 M NaCl. MD simulation for 50ns was performed with default settings.

5.10.3 IKK β in silico mutagenesis/docking

For mutating amino acid residues including SER181 and CYS179, we used the pymol mutagenesis plugin. Mutated structures were then simulated for 25ns using the protocol mentioned above. Simulated structures were then used in docking studies. For protein-ligand docking we used the same protocol mentioned previously, except in this case we focused only on the KD domain for interactions, since we knew that **7h** targets only the KD domain.

5.10.4 Covalent docking

Covalent docking was performed utilizing the covalent docking module (Glide) from the Schrodinger small molecule drug discovery suite. Ligands were first prepared using the Ligprep module and then used as an input for the covalent docking studies. For compounds **7h** and PTL, the reaction type was set to Michael addition to a double bond and for compounds DMAPT and **10** the reaction type was set to nucleophilic addition. Docking was performed using a Pose prediction (thorough) procedure with the minimization radius set to default. Scoring was performed using the MM-GBSA method. The top 10 poses were then ranked based on cDock affinity scores.

ACKNOWLEDGMENTS

We are grateful for the support provided by the NIH/National Cancer Institute (grant # R01 CA158275), the NIH/National Institute of Aging (grant # P01 AG012411), the NIH/National Institute of General Medical Sciences (grant # P20 GM109005), the Arkansas Research Alliance for an Arkansas Scholar award (to PAC), and to the NCI drug-screening program. Funding for equipment/facilities used in this research was provided by the Center for Advanced Surface Engineering, under the National Science Foundation Grant No. IIA-1457888 and the Arkansas EPSCoR Program, ASSET III.

Appendix A. Supplementary data

Fig. S1, Table S1, Videos 1-3, ¹H and ¹³C NMR spectra, and HRMS can be found in the Supporting Information.

Conflict of interest statement

The authors declare the following competing financial interest(s): The University of Arkansas for Medical Sciences (UAMS) holds patents on the molecules described in this

FUNDING SOURCES

The NIH/National Cancer Institute (grant # R01 CA158275), the NIH/National Institute of Aging (grant # P01 AG012411) and the NIH/National Institute of General Medical Sciences (grant # P20 GM109005).

REFERENCES

- [1] D.W. Knight, Feverfew: chemistry and biological activity, *Nat. Prod. Rep.* 12 (1995) 271-276.
- [2] F. S. El-Ferally, Melampolides from *Magnolia grandiflora*, *Phytochemistry*. 23 (1984) 2372-2374.
- [3] V. Janganani, N.R. Penthala, N.R. Madadi, Z. Chen, P.A. Crooks, Anti-cancer activity of carbamate derivatives of melampomagnolide B, *Bioor. Med. Chem. Lett.* 24 (2014) 3499-3502.
- [4] V. Janganani, J. Ponder, C.T. Jordan, M.J. Borrelli, N.R. Penthala, P.A. Crooks, Dimers of Melampomagnolide B Exhibit Potent Anticancer Activity against Hematological and Solid Tumor Cells, *J. Med. Chem.* 58 (2015) 8896-8906.
- [5] S. Bommagani, J. Ponder, N.R. Penthala, V. Janganani, C.T. Jordan, M.J. Borrelli, P.A. Crooks, Indole carboxylic acid esters of melampomagnolide B are potent anticancer agents against both hematological and solid tumor cells, *Eur. J. Med. Chem.* 136 (2017) 393-405.
- [6] V. Janganani, J. Ponder, S. Thakkar, C.T. Jordan, P.A. Crooks, Succinamide derivatives of melampomagnolide B and their anti-cancer activities, *Bioorg. Med. Chem.* 25 (2017) 3694-3705.
- [7] P.M. Bork, M.L. Schmitz, M. Kuhnt, C. Escher, M. Heinrich, Sesquiterpene lactone containing Mexican Indian medicinal plants and pure sesquiterpene lactones as potent inhibitors of transcription factor NF-kappaB, *FEBS Lett.* 402 (1997) 85-90.
- [8] S.P. Hehner, M. Heinrich, P.M. Bork, M. Vogt, F. Ratter, V. Lehmann, K. Schulze-Osthoff, W. Droge, M.L. Schmitz, Sesquiterpene lactones specifically inhibit activation of NF-kappa B by preventing the degradation of I kappa B-alpha and I kappa B-beta, *J. Biol. Chem.* 273 (1998) 1288-1297.
- [9] S. Nasim, S. Pei, F.K. Hagen, C.T. Jordan, P.A. Crooks, Melampomagnolide B: a new antileukemic sesquiterpene, *Bioorg. Med. Chem.* 19 (2011) 1515-1519.
- [10] M. Karin, Y. Cao, F.R. Greten, Z.W. Li, NF-kappaB in cancer: from innocent bystander to major culprit, *Nat. Rev. Cancer.* 2 (2002) 301-310.
- [11] D. Oka, K. Nishimura, M. Shiba, Y. Nakai, Y. Arai, M. Nakayama, H. Takayama, H. Inoue, A. Okuyama, N. Nonomura, Sesquiterpene lactone parthenolide suppresses tumor growth in a xenograft model of renal cell carcinoma by inhibiting the activation of NF-kappaB, *Int. J. Cancer.* 120 (2007) 2576-2581.
- [12] Y. Dai, M.L. Guzman, S. Chen, L. Wang, S.K. Yeung, X.Y. Pei, P. Dent, C.T. Jordan, S. Grant, The NF (Nuclear factor)-kappaB inhibitor parthenolide interacts with histone deacetylase inhibitors to induce MKK7/JNK1-dependent apoptosis in human acute myeloid leukaemia cells, *Br. J. Haematol.* 151 (2010) 70-83.
- [13] A. Paolicchi, S. Dominici, L. Pieri, E. Maellaro, A. Pompella, Glutathione catabolism as a signaling mechanism, *Biochem. Pharmacol.* 64 (2002) 1027-1035.
- [14] S. Pei, M. Minhajuddin, K.P. Callahan, M. Balys, J.M. Ashton, S.J. Neering, E.D. Lagadinou, C. Corbett, H. Ye, J.L. Liesveld, K.M. O'Dwyer, Z. Li, L. Shi, P. Greninger, J. Settleman, C. Benes, F.K. Hagen, J. Munger, P.A. Crooks, M.W. Becker, C.T. Jordan, Targeting aberrant glutathione metabolism to eradicate human acute myelogenous leukemia cells, *J. Biol. Chem.* 288 (2013) 33542-33558.
- [15] M.L. Guzman, R.M. Rossi, L. Karnischky, X. Li, D.R. Peterson, D.S. Howard, C.T. Jordan, The sesquiterpene lactone parthenolide induces apoptosis of human acute myelogenous leukemia stem and progenitor cells, *Blood.* 105 (2005) 4163-4169.

- [16] M.L. Guzman, R.M. Rossi, S. Neelakantan, X. Li, C.A. Corbett, D.C. Hassane, M.W. Becker, J.M. Bennett, E. Sullivan, J.L. Lachowicz, A. Vaughan, C.J. Sweeney, W. Matthews, M. Carroll, J.L. Liesveld, P.A. Crooks, C.T. Jordan, An orally bioavailable parthenolide analog selectively eradicates acute myelogenous leukemia stem and progenitor cells, *Blood*. 110 (2007) 4427-4435.
- [17] S. Neelakantan, S. Nasim, M.L. Guzman, C.T. Jordan, P.A. Crooks, Aminoparthenolides as novel anti-leukemic agents: Discovery of the NF-kappaB inhibitor, DMAPT (LC-1), *Bioorg. Med. Chem. Lett.* 19 (2009) 4346-4349.
- [18] S. Nasim, P.A. Crooks, Antileukemic activity of aminoparthenolide analogs, *Bioorg. Med. Chem. Lett.* 18 (2008) 3870-3873.
- [19] J.R. Woods, H. Mo, A.A. Bieberich, T. Alavanja, D.A. Colby, Fluorinated amino-derivatives of the sesquiterpene lactone, parthenolide, as (19)f NMR probes in deuterium-free environments, *J. Med. Chem.* 54 (2011) 7934-7941.
- [20] F.A. Macías., J.C.G. Galindo., G.M. Massanet., Potential allelopathic activity of several sesquiterpene lactone models, *Phytochemistry*. 31 (1992) 1969-1977.
- [21] Z.A. Albayati, V. Janganani, Z. Chen, J. Ponder, P.J. Breen, C.T. Jordan, P.A. Crooks, Identification of a melampomagnolide B analog as a potential lead molecule for treatment of acute myelogenous leukemia, *Bioorg. Med. Chem.* 25 (2017) 1235-1241.
- [22] P. Thirumurugan, D. Matosiuk, K. Jozwiak, Click chemistry for drug development and diverse chemical-biology applications, *Chem. Rev.* 113 (2013) 4905-4979.
- [23] G.C. Tron, T. Pirali, R.A. Billington, P.L. Canonico, G. Sorba, A.A. Genazzani, Click chemistry reactions in medicinal chemistry: applications of the 1,3-dipolar cycloaddition between azides and alkynes, *Med. Res. Rev.* 28 (2008) 278-308.
- [24] H.C. Kolb, M.G. Finn, K.B. Sharpless, Click Chemistry: Diverse Chemical Function from a Few Good Reactions, *Angew. Chem. Int. Ed. Engl.* 40 (2001) 2004-2021.
- [25] H.C. Kolb, K.B. Sharpless, The growing impact of click chemistry on drug discovery, *Drug. Discov. Today*. 8 (2003) 1128-1137.
- [26] J.E. Moses, A.D. Moorhouse, The growing applications of click chemistry, *Chem. Soc. Rev.* 36 (2007) 1249-1262.
- [27] N. Kuntala, J.R. Telu, V. Banothu, S.B. Nallapati, J.S. Anireddy, S. Pal, Novel benzoxepine-1,2,3-triazole hybrids: synthesis and pharmacological evaluation as potential antibacterial and anticancer agents, *Med. Chem. Comm.* 6 (2015) 1612-1619.
- [28] C. Bengtsson, A.E. Lindgren, H. Uvell, F. Almqvist, Design, synthesis and evaluation of triazole functionalized ring-fused 2-pyridones as antibacterial agents, *Eur. J. Med. Chem.* 54 (2012) 637-646.
- [29] P.M. Chaudhary, S.R. Chavan, F. Shirazi, M. Razdan, P. Nimkar, S.P. Maybhate, A.P. Likhite, R. Gonnade, B.G. Hazara, M.V. Deshpande, S.R. Deshpande, Exploration of click reaction for the synthesis of modified nucleosides as chitin synthase inhibitors, *Bioorg. Med. Chem.* 17 (2009) 2433-2440.
- [30] N. Dubey, M. C. Sharma, A. Kumar, P. Sharma, A click chemistry strategy to synthesize geraniol-coupled 1,4-disubstituted 1,2,3-triazoles and exploration of their microbiocidal and antioxidant potential with molecular docking profile, *Med. Chem. Res.* 24 (2015) 2717-2731.
- [31] H. Cheng, J. Wan, M.I. Lin, Y. Liu, X. Lu, J. Liu, Y. Xu, J. Chen, Z. Tu, Y.S. Cheng, K. Ding, Design, synthesis, and in vitro biological evaluation of 1H-1,2,3-triazole-4-carboxamide derivatives as new anti-influenza A agents targeting virus nucleoprotein, *J. Med. Chem.* 55 (2012) 2144-2153.
- [32] S.K. Vernekar, L. Qiu, J. Zhang, J. Kankanala, H. Li, R.J. Geraghty, Z. Wang, 5'-Silylated 3'-1,2,3-triazolyl Thymidine Analogues as Inhibitors of West Nile Virus and Dengue Virus, *J. Med. Chem.* 58 (2015) 4016-4028.
- [33] T.W. Kim, Y. Yong, S.Y. Shin, H. Jung, K.H. Park, Y.H. Lee, Y. Lim, K.Y. Jung, Synthesis and biological evaluation of phenyl-1H-1,2,3-triazole derivatives as anti-inflammatory agents, *Bioorg. Chem.* 59 (2015) 1-11.
- [34] S. Haider, M.S. Alam, H. Hamid, S. Shafi, A. Nargotra, P. Mahajan, S. Nazreen, A.M. Kalle, C. Kharbanda, Y. Ali, A. Alam, A.K. Panda, Synthesis of novel 1,2,3-triazole based benzoxazolinones: their TNF-alpha based molecular docking with in-vivo anti-inflammatory, antinociceptive activities and ulcerogenic risk evaluation, *Eur. J. Med. Chem.* 70 (2013) 579-588.
- [35] V.G. Reddy, S.R. Bonam, T.S. Reddy, R. Akunuri, V.G.M. Naidu, V.L. Nayak, S.K. Bhargava, H.M.S. Kumar, P. Srihari, A. Kamal, 4beta-amidotriazole linked podophyllotoxin congeners: DNA topoisomerase-IIalpha inhibition and potential anticancer agents for prostate cancer, *Eur. J. Med. Chem.* 144 (2018) 595-611.
- [36] T. Srinivasa Reddy, H. Kulhari, V. Ganga Reddy, A.V. Subba Rao, V. Bansal, A. Kamal, R. Shukla, Synthesis and biological evaluation of pyrazolo-triazole hybrids as cytotoxic and apoptosis inducing agents, *Org. Biomol. Chem.* 13 (2015) 10136-10149.
- [37] K.R. Senwar, P. Sharma, T.S. Reddy, M.K. Jeengar, V.L. Nayak, V.G. Naidu, A. Kamal, N. Shankaraiah, Spirooxindole-derived morpholine-fused-1,2,3-triazoles: Design, synthesis, cytotoxicity and apoptosis inducing studies, *Eur. J. Med. Chem.* 102 (2015) 413-424.
- [38] N.R. Penthala, L. Madhukuri, S. Thakkar, N.R. Madadi, G. Lamture, R.L. Eoff, P.A. Crooks, Synthesis and anti-cancer screening of novel heterocyclic-(2H)-1,2,3-triazoles as potential anti-cancer agents, *Med.Chem.Comm.* 6 (2015) 1535-1543.
- [39] N.R. Madadi, N.R. Penthala, K. Howk, A. Ketkar, R.L. Eoff, M.J. Borrelli, P.A. Crooks, Synthesis and biological evaluation of novel 4,5-disubstituted 2H-1,2,3-triazoles as cis-constrained analogues of combretastatin A-4, *Eur. J. Med. Chem.* 103 (2015) 123-132.
- [40] J.A. Stefely, R. Palchadhuri, P.A. Miller, R.J. Peterson, G.C. Moraski, P.J. Hergenrother, M.J. Miller, N-((1-benzyl-1H-1,2,3-triazol-4-yl)methyl)arylamide as a new scaffold that provides rapid access to antimicrotubule agents: synthesis and evaluation of antiproliferative activity against select cancer cell lines, *J. Med. Chem.* 53 (2010) 3389-3395.
- [41] Y. Bourne, H.C. Kolb, Z. Radic, K.B. Sharpless, P. Taylor, P. Marchot, Freeze-frame inhibitor captures acetylcholinesterase in a unique conformation, *Proc. Natl. Acad. Sci. U S A.* 101 (2004) 1449-1454.
- [42] E. Bonandi, M.S. Christodoulou, G. Fumagalli, D. Perdicchia, G. Rastelli, D. Passarella, The 1,2,3-triazole ring as a bioisostere in medicinal chemistry, *Drug. Discov. Today*. 22 (2017) 1572-1581.
- [43] W.S. Horne, M.K. Yadav, C.D. Stout, M.R. Ghadiri, Heterocyclic peptide backbone modifications in an alpha-helical coiled coil, *J. Am. Chem. Soc.* 126 (2004) 15366-15367.
- [44] A. Kamal, N. Shankaraiah, C.R. Reddy, S. Prabhakar, N. Markandeya, H.K. Srivastava, G.N. Sastry, Synthesis of bis-1,2,3-triazolo-bridged unsymmetrical pyrrolobenzodiazepine trimers via 'click' chemistry and their DNA-binding studies, *Tetrahedron*. 66 (2010) 5498-5506.
- [45] H. Li, R. Aneja, I. Chaiken, Click chemistry in peptide-based drug design, *Molecules*. 18 (2013) 9797-9817.
- [46] Y.L. Angell, K. Burgess, Peptidomimetics via copper-catalyzed azide-alkyne cycloadditions, *Chem. Soc. Rev.* 36 (2007) 1674-1689.
- [47] D. Dheer, V. Singh, R. Shankar, Medicinal attributes of 1,2,3-triazoles: Current developments, *Bioorg. Chem.* 71 (2017) 30-54.
- [48] R. Galli, E. Binda, U. Orfanelli, B. Cipelletti, A. Gritti, S. De Vitis, R. Fiocco, C. Foroni, F. Dimeco, A. Vescovi, Isolation and characterization of tumorigenic, stem-like neural precursors from human glioblastoma, *Cancer. Res.* 64 (2004) 7011-7021.
- [49] K.Y. Yeung, A. Dickinson, J.F. Donoghue, G. Polekhina, S.J. White, D.K. Grammatopoulos, M. McKenzie, T.G. Johns, J.C. St John, The identification of mitochondrial DNA variants in

- glioblastoma multiforme, *Acta. Neuropathol. Commun.* 2 (2014) 1.
- [50] P. Bhat-Nakshatri, T.R. Newton, R. Goulet, Jr., H. Nakshatri, NF-kappaB activation and interleukin 6 production in fibroblasts by estrogen receptor-negative breast cancer cell-derived interleukin 1alpha, *Proc. Natl. Acad. Sci. U S A.* 95 (1998) 6971-6976.
- [51] M. Adli, E. Merkhofer, P. Cogswell, A.S. Baldwin, IKKalpha and IKKbeta each function to regulate NF-kappaB activation in the TNF-induced/canonical pathway, *PLoS One.* 5 (2010) e9428.
- [52] E.D. Tang, N. Inohara, C.Y. Wang, G. Nunez, K.L. Guan, Roles for homotypic interactions and transautophosphorylation in IkappaB kinase beta (IKKbeta) activation [corrected], *J. Biol. Chem.* 278 (2003) 38566-38570.
- [53] A. Israel, The IKK complex, a central regulator of NF-kappaB activation, *Cold. Spring. Harb. Perspect. Biol.* 2 (2010) a000158.
- [54] A. Oeckinghaus, M.S. Hayden, S. Ghosh, Crosstalk in NF-kappaB signaling pathways, *Nat. Immunol.* 12 (2011) 695-708.
- [55] G. Ghosh, V.Y. Wang, D.B. Huang, A. Fusco, NF-kappaB regulation: lessons from structures, *Immunol. Rev.* 246 (2012) 36-58.
- [56] M. Hinz, C. Scheidereit, The IkappaB kinase complex in NF-kappaB regulation and beyond, *EMBO. Rep.* 15 (2014) 46-61.
- [57] S. Polley, D.B. Huang, A.V. Hauenstein, A.J. Fusco, X. Zhong, D. Vu, B. Schrofelbauer, Y. Kim, A. Hoffmann, I.M. Verma, G. Ghosh, T. Huxford, A structural basis for IkappaB kinase 2 activation via oligomerization-dependent trans autophosphorylation, *PLoS. Biol.* 11 (2013) e1001581.
- [58] Q. Li, D. Van Antwerp, F. Mercurio, K.F. Lee, I.M. Verma, Severe liver degeneration in mice lacking the IkappaB kinase 2 gene, *Science.* 284 (1999) 321-325.
- [59] Z.W. Li, W. Chu, Y. Hu, M. Delhase, T. Deerinck, M. Ellisman, R. Johnson, M. Karin, The IKKbeta subunit of IkappaB kinase (IKK) is essential for nuclear factor kappaB activation and prevention of apoptosis, *J. Exp. Med.* 189 (1999) 1839-1845.
- [60] A. Salmeron, J. Janzen, Y. Soneji, N. Bump, J. Kamens, H. Allen, S.C. Ley, Direct phosphorylation of NF-kappaB1 p105 by the IkappaB kinase complex on serine 927 is essential for signal-induced p105 proteolysis, *J. Biol. Chem.* 276 (2001) 22215-22222.
- [61] M.J. May, S.E. Larsen, J.H. Shim, L.A. Madge, S. Ghosh, A novel ubiquitin-like domain in IkappaB kinase beta is required for functional activity of the kinase, *J. Biol. Chem.* 279 (2004) 45528-45539.
- [62] G. Xu, Y.C. Lo, Q. Li, G. Napolitano, X. Wu, X. Jiang, M. Dreano, M. Karin, H. Wu, Crystal structure of inhibitor of kappaB kinase beta, *Nature.* 472 (2011) 325-330.
- [63] S. Dai, T. Hirayama, S. Abbas, Y. Abu-Amer, The IkappaB kinase (IKK) inhibitor, NEMO-binding domain peptide, blocks osteoclastogenesis and bone erosion in inflammatory arthritis, *J. Biol. Chem.* 279 (2004) 37219-37222.
- [64] J. Yang, R. Yan, A. Roy, D. Xu, J. Poisson, Y. Zhang, The I-TASSER Suite: protein structure and function prediction, *Nat. Methods.* 12 (2015) 7-8.
- [65] S. Liu, Y.R. Misquitta, A. Olland, M.A. Johnson, K.S. Kelleher, R. Kriz, L.L. Lin, M. Stahl, L. Mosyak, Crystal structure of a human IkappaB kinase beta asymmetric dimer, *J. Biol. Chem.* 288 (2013) 22758-22767.
- [66] O. Trott, A.J. Olson, AutoDock Vina: improving the speed and accuracy of docking with a new scoring function, efficient optimization, and multithreading, *J. Comput. Chem.* 31 (2010) 455-461.
- [67] R.A. Laskowski, M.B. Swindells, LigPlot+: multiple ligand-protein interaction diagrams for drug discovery, *J. Chem. Inf. Model.* 51 (2011) 2778-2786.
- [68] M.S. Byun, J. Choi, D.M. Jue, Cysteine-179 of IkappaB kinase beta plays a critical role in enzyme activation by promoting phosphorylation of activation loop serines, *Exp. Mol. Med.* 38 (2006) 546-552.
- [69] M.J. May, F. D'Acquisto, L.A. Madge, J. Glockner, J.S. Pober, S. Ghosh, Selective inhibition of NF-kappaB activation by a peptide that blocks the interaction of NEMO with the IkappaB kinase complex, *Science.* 289 (2000) 1550-1554.
- [70] A. Larabi, J.M. Devos, S.L. Ng, M.H. Nanao, A. Round, T. Maniatis, D. Panne, Crystal structure and mechanism of activation of TANK-binding kinase 1, *Cell. Rep.* 3 (2013) 734-746.
- [71] N.J. Lawrence, A.T. McGown, J. Nduka, J.A. Hadfield, R.G. Pritchard, Cytotoxic Michael-type amine adducts of alpha-methylene lactones alantolactone and isosalantolactone, *Bioorg. Med. Chem. Lett.* 11 (2001) 429-431.
- [72] D.R. Hwang, Y.S. Wu, C.W. Chang, T.W. Lien, W.C. Chen, U.K. Tan, J.T. Hsu, H.P. Hsieh, Synthesis and anti-viral activity of a series of sesquiterpene lactones and analogues in the subgenomic HCV replicon system, *Bioorg. Med. Chem.* 14 (2006) 83-91.
- [73] E. Hejchman, R.D. Haugwitz, M. Cushman, Synthesis and cytotoxicity of water-soluble ambrosin prodrug candidates, *J. Med. Chem.* 38 (1995) 3407-3410.
- [74] H. Matsuda, I. Toguchida, K. Ninomiya, T. Kageura, T. Morikawa, M. Yoshikawa, Effects of sesquiterpenes and amino acid-sesquiterpene conjugates from the roots of *Saussurea lappa* on inducible nitric oxide synthase and heat shock protein in lipopolysaccharide-activated macrophages, *Bioorg. Med. Chem.* 11 (2003) 709-715.
- [75] L.V. Rubinstein, R.H. Shoemaker, K.D. Paull, R.M. Simon, S. Tosini, P. Skehan, D.A. Scudiero, A. Monks, M.R. Boyd, Comparison of in vitro anticancer-drug-screening data generated with a tetrazolium assay versus a protein assay against a diverse panel of human tumor cell lines, *J. Natl. Cancer. Inst.* 82 (1990) 1113-1118.
- [76] P. Bhat-Nakshatri, C.P. Goswami, S. Badve, L. Magnani, M. Lupien, H. Nakshatri, Molecular Insights of Pathways Resulting from Two Common PIK3CA Mutations in Breast Cancer, *Cancer Research.* 76 (2016) 3989-4001.
- [77] A.C. Wallace, R.A. Laskowski, J.M. Thornton, LIGPLOT: a program to generate schematic diagrams of protein-ligand interactions, *Protein. Eng.* 8 (1995) 127-134.

- Design and synthesis of triazole derivatives of melampomagnolide B (MMB).
- Screening of MMB triazoles against hematological and solid tumor cell lines.
- MMB triazole inhibition of p65 and I κ B α phosphorylation, and NF- κ B binding to DNA
- Structural modeling of interaction of MMB triazoles with the IKK β protein subunit.

ACCEPTED MANUSCRIPT